AGU PUBLICATIONS

Geochemistry, Geophysics, Geosystems

RESEARCH ARTICLE
10.1002/2014GC005458

Special Section:
Lithospheric Evolution of Cenozoic UHP Terranes: From Convergence to Extension

Key Points:
- GPS reveals crustal deformation and microplate kinematics in the Woodlark Basin, SE Papua New Guinea
- Exhumation of UHP rocks in southeastern PNG is associated with active crustal extension
- Our results demonstrate that low-angle normal faults can slip at rates of several mm/yr or more

Correspondence to:
L. M. Wallace,
lwallace@utexas.edu

Citation:
Wallace, L. M., S. Ellis, T. Little, P. Tregoning, N. Palmer, R. Rosa, R. Stanaway, J. Oa, E. Nidkombu, and J. Kwazi (2014), Continental breakup and UHP rock exhumation in action: GPS results from the Woodlark Rift, Papua New Guinea, *Geochem. Geophys. Geosyst.*, *15*, 4267–4290, doi:10.1002/2014GC005458.

Received 13 JUN 2014
Accepted 16 OCT 2014
Accepted article online 23 OCT 2014
Published online 11 NOV 2014

Continental breakup and UHP rock exhumation in action: GPS results from the Woodlark Rift, Papua New Guinea

Laura M. Wallace[1], Susan Ellis[2], Tim Little[3], Paul Tregoning[4], Neville Palmer[2], Robert Rosa[5], Richard Stanaway[6], John Oa[7], Edwin Nidkombu[7], and John Kwazi[7]

[1]Institute for Geophysics, University of Texas, Austin, Texas, USA, [2]GNS Science, Lower Hutt, New Zealand, [3]School of Geography, Environment, and Earth Sciences, Victoria University of Wellington, Wellington, New Zealand, [4]Research School for the Earth Sciences, Australian National University, Canberra, ACT, Australia, [5]Surveying Department, University of Technology, Lae, Papua New Guinea, [6]Quickclose Pty. Ltd., Carlton, Victoria, Australia, [7]PNG National Mapping Bureau, Port Moresby, Papua New Guinea

Abstract We show results from a network of campaign Global Positioning System (GPS) sites in the Woodlark Rift, southeastern Papua New Guinea, in a transition from seafloor spreading to continental rifting. GPS velocities indicate anticlockwise rotation (at 2–2.7°/Myr, relative to Australia) of crustal blocks north of the rift, producing 10–15 mm/yr of extension in the continental rift, increasing to 20–40 mm/yr of seafloor spreading at the Woodlark Spreading Center. Extension in the continental rift is distributed among multiple structures. These data demonstrate that low-angle normal faults in the continents, such as the Mai'iu Fault, can slip at high rates nearing 10 mm/yr. Extensional deformation observed in the D'Entrecasteaux Islands, the site of the world's only actively exhuming Ultra-High Pressure (UHP) rock terrane, supports the idea that extensional processes play a critical role in UHP rock exhumation. GPS data do not require significant interseismic coupling on faults in the region, suggesting that much of the deformation may be aseismic. Westward transfer of deformation from the Woodlark Spreading Center to the main plate boundary fault in the continental rift (the Mai'iu fault) is accommodated by clockwise rotation of a tectonic block beneath Goodenough Bay, and by dextral strike slip on transfer faults within (and surrounding) Normanby Island. Contemporary extension rates in the Woodlark Spreading Center are 30–50% slower than those from seafloor spreading-derived magnetic anomalies. The 0.5 Ma to present seafloor spreading estimates for the Woodlark Basin may be overestimated, and a reevaluation of these data in the context of the GPS rates is warranted.

1. Introduction

Continental breakup leads to the formation of ocean basins, and is among the most important, but least understood processes in plate tectonics. The Woodlark Rift in southeastern Papua New Guinea, the East African Rift, and the Gulf of California are among only a few places on Earth where continental breakup just prior to seafloor spreading is well expressed in the present day, and where active processes associated with breakup can be measured in real time. Measurement of crustal strain rates and the kinematics of actively rifting plate boundaries been revolutionized by the development and increasing use of GPS methods over the last 20 years [e.g., *Jónsson et al*., 1997; *Niemi et al*., 2004; *Bendick et al*., 2006; *Hreinsdottir et al*., 2009, to name only a few]. GPS methods to determine crustal deformation can be used to address many of the outstanding questions concerning continental rifting processes. For example, does active continental rifting prior to full-blown seafloor spreading occur over a broad region, and if so, how does it eventually coalesce into a narrow zone of seafloor spreading [e.g., *Taylor et al*., 1999]? How much of the rifting is accommodated by faulting versus magmatism, and what role does lower crustal flow play [e.g., *White and McKenzie*, 1989; *van Wijk et al*., 2001; *Buck*, 2006, 2007; *Little et al*., 2011; *Bialas et al*., 2010]? Why do some extensional regions experience asymmetric rifting, with development of weak, low-angle faults, and core complexes, while others are more symmetric and contain an abundance of steeper-dipping, lower displacement normal faults? How much of the overall extension budget at different locations is accommodated by deformation in the upper versus the lower crust? Although many studies treat continental breakup as a two-dimensional process, what role does the third dimension play in propagation of rifting and seafloor spreading [e.g., *van Wijk and Blackman*, 2005; *Ellis et al*., 2011]?

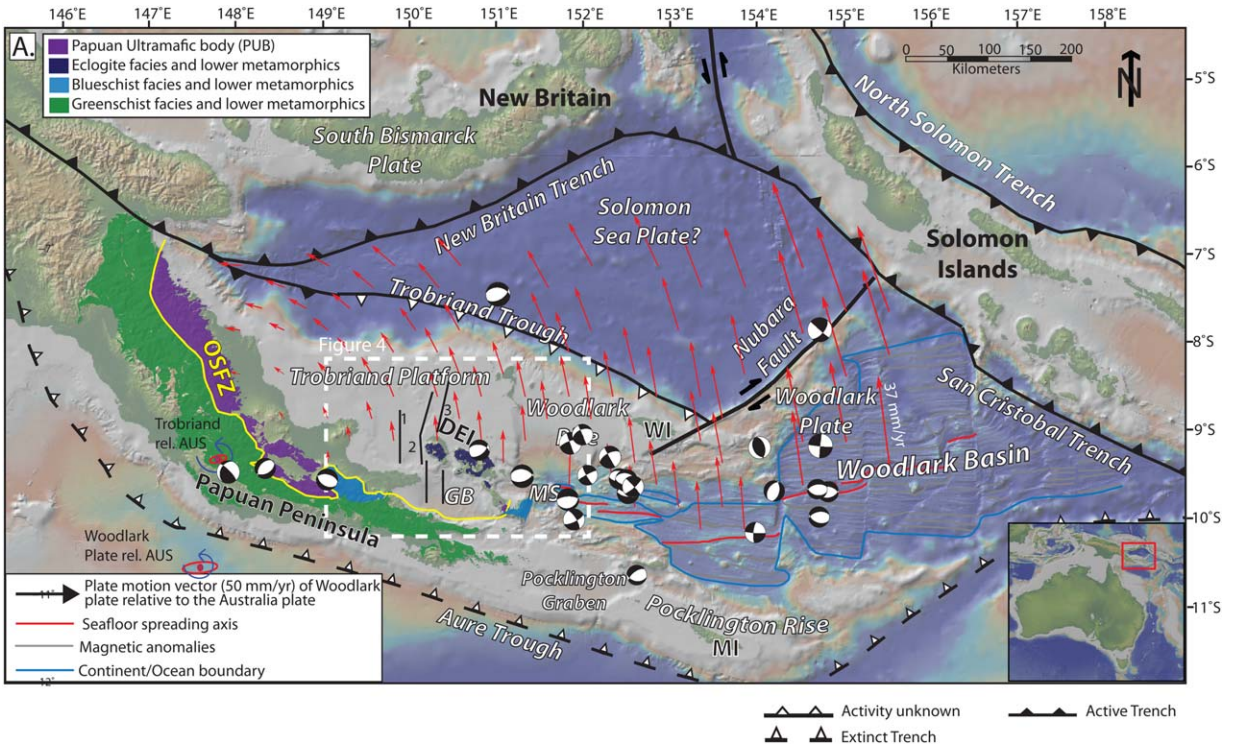

Figure 1. Tectonic setting of the Woodlark Rift. Basemap modified from *Fitz and Mann* [2013a]. Red vectors show rotation of the Woodlark Plate and Trobriand Block about poles of rotation from this study (poles shown on left-hand side, labeled). Earthquake focal mechanisms for the Woodlark Rift from are shown for events shallower than 50 km, from 1976 to present (Global CMT Project) [*Dziewonski et al*., 1981; *Ekstrom et al*., 2012]. Lines labeled 1, 2, and 3 near the D'Entrecasteaux Islands show the locations of the structural profiles used by *Fitz and Mann* [2013a] that are discussed in section 5.1. DEI = D'Entrecasteaux Islands, WI = Woodlark Island, GB = Goodenough Bay; MI = Misima Island; OSFZ = Owen Stanley Fault Zone; MS = Moresby Seamount.

Extension in the Woodlark Basin in southeastern Papua New Guinea accommodates northward motion of the Woodlark Plate relative to the Australian Plate. In the eastern Woodlark Basin, well-developed seafloor spreading has been ongoing for at least the last 3.6 Ma, and probably longer (east of 151.5°E) [*Taylor et al*., 1999], while in the western portion (e.g., the Woodlark rift; west of 151.5°E), active continental rifting has not yet given way to seafloor spreading (Figure 1). As well as exemplifying recent along-strike continental breakup, a key aspect of the Woodlark Rift is that this zone of continental extension has hosted exhumation of the world's youngest known Ultra-High Pressure (UHP) rocks [e.g., *Baldwin et al*., 2004, 2008; *Gordon et al*., 2012]. This makes the Woodlark Rift the only place on Earth where one can quantify the tectonic boundary conditions associated with active UHP rock exhumation, as all other well-studied UHP terranes on earth were exposed many tens of millions of years ago [e.g., *Hacker*, 2007; *Epard and Steck*, 2008; *Stearns et al*., 2013]. Moreover, the Woodlark Rift is known to be the site of active, low-angle normal faulting (LANF) [*Abers et al*., 1997; *Abers*, 2001; *Spencer*, 2010; *Colletini*, 2011; *Daczko et al*., 2011]. GPS provides an opportunity to constrain slip rates on active LANFs. Here, we show results of a network of ~40 campaign GPS sites in the Woodlark Rift region measured between 2009 and 2012, augmented by some earlier measurements (1996–2008) at several of the sites. The GPS results reveal the detailed distribution of deformation within the continental portion of the Woodlark Rift, as well as the kinematics of microplate rotation and rates of modern-day rifting across the region. Rates of rifting from the GPS network are approximately half to two-thirds of the seafloor spreading rates determined from magnetic anomalies. The GPS results show that individual normal faults are slipping at rates on the order of 10–19 mm/yr—the fastest such rates for active normal faults documented anywhere in the world [cf. *Mouslopolou et al*., 2009].

2. Tectonic Setting

The Australian and Pacific Plates converge obliquely at 10–11 cm/yr across the Papua New Guinea (PNG) region (Figure 1). As a consequence of the rapid and complex nature of the plate interactions there, PNG

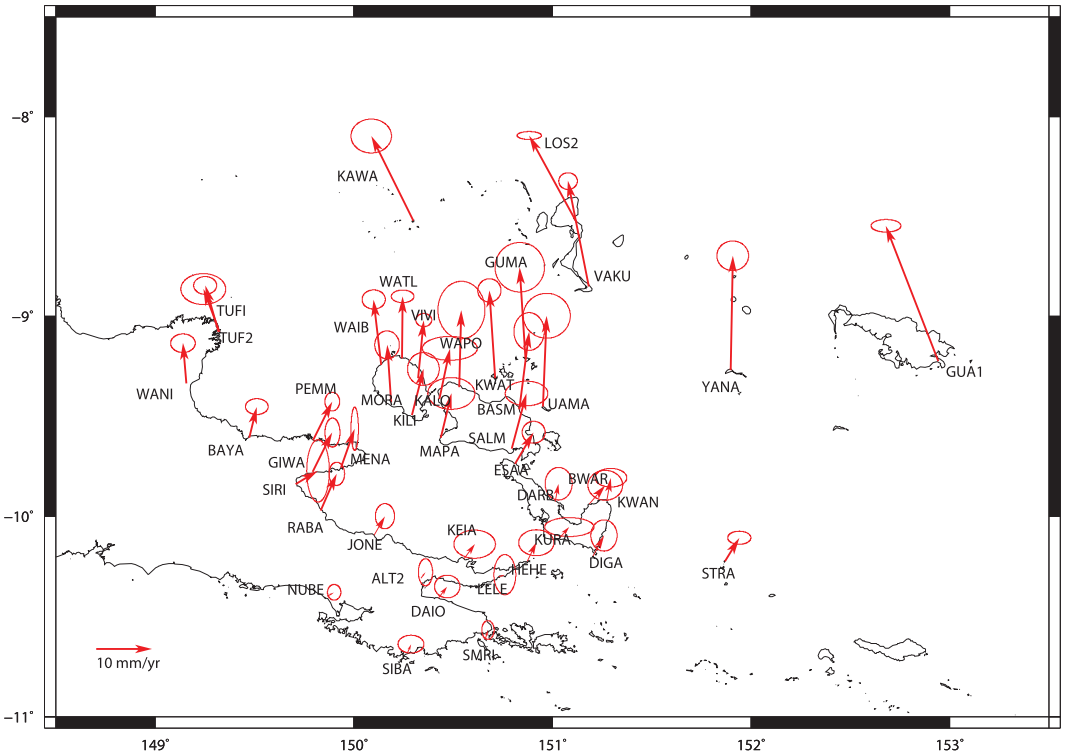

Figure 2. GPS velocities from this study shown relative to the Australian Plate. Scale arrow shown in bottom left. Uncertainty ellipses are 95% confidence.

has been fragmented into an array of microplates that are rapidly rotating with respect to one another [*Tregoning et al*., 1998; *Wallace et al*., 2004]. One of these is the Woodlark Plate, which comprises much of SE PNG; the Woodlark Plate rotates counter clockwise relative to the Australian Plate about a nearby pole of rotation (Figure 1) [*Taylor et al*., 1999; *Tregoning et al*., 1998; *Wallace et al*., 2004]. Seafloor spreading has occurred in the eastern Woodlark Basin (east of ∼151.5°E) at rates >20–60 mm/yr since ∼6–3.6 Ma, whereas the onset of continental rifting in the region is suggested by some to have begun slightly earlier, ∼8 Ma [*Taylor et al*., 1999; *Taylor and Huchon*, 2002]. The western, continental portion of this zone of extension is called the Woodlark Rift, and today it undergoes lower rates of extension (<10–20 mm/yr; *Tregoning et al*., 1998; *Wallace et al*., 2004] than the seafloor spreading portion to the east (the Woodlark Spreading Center) [*Taylor et al*., 1999].

Several key features define the western Woodlark Rift as continental: (1) crustal thicknesses >20–30 km in the center of the rift [*Abers et al*., 2002], (2) *P* wave velocities of 5.6–6.9 km/s at 10–25 km depth [*Ferris et al*., 2006] indicating crust of a bulk felsic to intermediate composition, (3) a volumetric dominance of quartzofeldspathic lithologies and granitoids in the surface geology [*Davies and Warren*, 1988; *Little et al*., 2007, 2011, 2013; *Davies*, 2012]. Some mafic rocks are found in the continental rift, but they are not volumetrically significant. The Woodlark Rift contains several Metamorphic Core Complexes (MCCs), including eclogite-bearing gneiss domes of the D'Entrecasteaux Islands (DEI, Figure 1), as well as active volcanic centers and normal faults [*Smith and Davies*, 1976; *Abers et al*., 1997; *Taylor and Huchon*, 2002; *Little et al*., 2007, 2011; *Fitz and Mann*, 2013a].

A large portion of the continental rifting in southeast PNG is accommodated by slip on normal faults, most of them submerged or bounding the flanks of the up to 2.5 km high, subaerially exhumed gneiss domes of the D'Entrecasteaux Islands (Figure 4) [*Hill*, 1994; *Fitz and Mann*, 2013a; *Little et al*., 2007, 2011]. The Mai'iu Fault (also called the Owen Stanley Fault by *Fitz and Mann* [2013a]) is part of the Owen Stanley Fault Zone and separates the Australian Plate derived Owen-Stanley metamorphics (and some ophiolitic rocks that rest structurally above them), to the SW, from Woodlark Plate rocks that consist of Cretaceous-Paleogene ophiolitic and arc-related basement rocks, and their Neogene-Recent sedimentary and volcanic cover, to the NE. It is thought to be the most active fault in the Woodlark Rift (Figure 1). The Mai'iu Fault extends along the

southern margin of the rift from the Dayman Dome for >100 km to the southeast, along the south side of Goodenough Bay (Figures 1 and 2) [*Smith and Davies*, 1976]. Given its high rainfall, mountainous setting, the ~25 km width, >2800 m height, and smooth, domal, and corrugated nature of the scarp exhumed along this fault are evidence of rapid and very recent exhumation along an active normal fault [e.g., *Ollier and Pain*, 1980; *Spencer*, 2010; *Fitz and Mann*, 2013b]. Uplifted Pleistocene coral reefs along the south coast of Goodenough Bay on the footwall of the Mai'iu/Goodenough Bay Fault indicate footwall uplift rates of 1–4 mm/yr (increasing to the NW) [*Fitz and Mann*, 2013b] (F. Taylor, personal communication, 2013), whereas up to 5 km of Pliocene-Recent sediments downdropped and back-tilted immediately offshore of the trace indicate hanging wall subsidence [*Fitz and Mann*, 2013b]—observations that are also consistent with slip rates on this fault being high, at least several mm/yr or more.

The Cenozoic geological history of southeastern PNG region is complex. Most of the Papuan Peninsula and D'Entrecasteaux Islands are composed of the Papuan Orogen, which evolved during Paleogene collision between the Australian continent and an island arc terrane to the north [*Davies and Jaques*, 1984; *van Ufford and Cloos*, 2005]. During this collision, the Papuan Ultramafic Belt (PUB, Figure 1) was obducted southwestward onto the subducting Australian Plate (Owen Stanley Metamorphics), beginning by ~58 Ma [*Lus et al*., 2004]. Collision continued until the early Miocene, based on Ar/Ar and K/Ar ages on amphibole and white mica in the Owen Stanley metamorphics in the Papuan Peninsula being as young as 24–22 Myr [*Davies and Jaques*, 1984; *Davies and Williamson*, 1998]. It is less clear what happened following the cessation of arc continent collision. Many workers have suggested that southward subduction of the Solomon Sea oceanic lithosphere initiated on the Trobriand Trough (Figure 1) [*Davies et al*., 1987; *Taylor et al*., 1999; *Taylor and Huchon*, 2002], leading to the Miocene onset of arc volcanism across the Papuan Peninsula and D'Entrecasteaux Islands [*Dow*, 1977; *Smith*, 1982; *Smith and Milsom*, 1984; *van Ufford and Cloos*, 2005]. There is little to no evidence for active subduction (or a subducted slab) at the Trobriand Trough today [*Abers and Roecker*, 1991; *Kirchoff-Stein*, 1992; *Hall and Spakman*, 2002; *Abers et al*., 2002], indicating that if subduction at the Trobriand Trough occurred in the past, it likely ceased sometime in the Miocene or Pliocene.

Stratigraphic evidence from drill holes for a widespread marine inundation at ~8.4 Ma has been cited to mark the onset of Woodlark rifting [*Taylor et al*., 1999; *Taylor and Huchon*, 2002]. Seafloor spreading began in the eastern Woodlark Basin by ~6 Ma, and has propagated westward at a rate of ~140 km/Myr [*Taylor and Exon*, 1987]. The current tip of seafloor spreading is located at ~151.5°E, near the Moresby Seamount (Figures 1 and 4) [*Taylor et al*., 1999]. There is a strong change in seismic velocities on either side of the current rift tip, consistent with slower continental crust west of the tip, and faster oceanic crust east of it, suggesting that the transition from continental rifting to seafloor spreading occurs over a very narrow zone [*Ferris et al*., 2006]. Shear wave splitting to image anisotropy beneath the continental portion of the rift shows that fast directions are parallel to the extension direction, similar to what is observed at mid-ocean ridges, and in contrast to other continental rifts that tend to have rift axes parallel to fast directions [*Eilon et al*., 2014]. *Eilon et al*. [2014] suggested that the magnitude of extension in the continental portion of the Woodlark rift has been large enough to produce a mantle fabric similar to that of mid-ocean ridges, in contrast to less extended continental rifts elsewhere.

Between 6 and 0.5 Ma, most of the Woodlark seafloor spreading can be described by a pole of rotation at 147°E, 9.3°S, with anticlockwise rotation of the Woodlark Plate relative to the Australian Plate at a rate of 4.23°/Myr (Figure 1) [*Goodliffe*, 1998; *Taylor et al*., 1999]. *Goodliffe et al*. [1997] document a reorientation of spreading center segments at ~80 ka, in response to a shift in the Euler pole for Woodlark-Australia spreading at ~0.5 Ma. Based on magnetic anomalies, the 0.5 Ma to present Euler pole for Woodlark spreading is southwest of the earlier rotation pole, near 144°E, 12°S, with a slower anticlockwise rotation rate of 2.4°/Ma [*Goodliffe*, 1998], producing total spreading rates of ~4 cm/yr near 152°E, increasing to 5.6 cm/yr near 156°E in the eastern Woodlark Basin.

Gneiss domes in the D'Entrecasteaux Islands (Figure 1) contain the world's youngest Ultra-High Pressure (UHP, eclogite-facies) rocks. In these domes, eclogite-facies assemblages have been dated at 5–8 Ma; and retrogressive, amphibolite-facies assemblages at ~2.5–3.5 Ma—results that indicate exhumation at rates of 2–3 cm/yr from >40 to 90 km depths [*Baldwin et al*., 2004, 2008; *Gordon et al*., 2012]. The UHP terranes were derived from a previously thinned, and mostly Cretaceous age part of the Australian margin that was subducted northeastward beneath the Papuan ophiolite and arc during the Papuan collision [*Davies and Jaques*, 1984; *Davies and Warren*, 1992; *Zirakparvar et al*., 2013]. It is enigmatic, however, that the Late

Table 1. GPS Sites, Location (Longitude/Latitude), ITRF2008 Velocities (mm/yr), Australian Plate-Fixed Velocities, and Uncertainties (mm/yr)[a]

Site	Longitude	Latitude	V_e (IT08; mm/yr)	V_n (IT08; mm/yr)	V_e (AUS-fix; mm/yr)	V_n (AUS-fix; mm/yr)	σ_e	σ_n
*ALIC	133.886	−23.67	32.32	59.66	0.21	0.13	0.38	0.35
ALT2	150.338	−10.31	33.54	56.81	0.82	1.08	0.52	0.99
BASM	150.833	−9.466	34.82	69.45	1.77	13.91	1.11	1.38
BAYA	149.474	−9.608	34.55	61.59	1.35	5.55	0.83	0.58
BWAR	151.185	−9.94	35.65	58.77	2.89	3.37	1.27	1.09
*CEDU	133.81	−31.867	28.92	59.04	−0.14	−0.49	0.52	0.46
*CHAT	183.434	−43.956	−40.68	33.25	−33.83	−1.71	0.12	0.2
*CKIS	200.199	−21.201	−62.97	36.18	−77.21	16.67	0.55	0.65
DAIO	150.427	−10.408	34.21	57.73	1.55	2.04	0.93	0.83
DARB	151.015	−9.927	33.37	58.65	0.58	3.18	0.99	1.19
DARW	131.133	−12.844	35.76	60.03	−0.04	0.34	0.38	0.43
DIGA	151.204	−10.2	34.61	59.11	1.98	3.71	0.96	1.14
ESAA	150.812	−9.739	36.25	61.2	3.33	5.65	0.84	0.8
GIWA	149.794	−9.78	36.58	63	3.51	7.07	0.55	1.06
GUA1	152.944	−9.225	23.44	78.9	−9.4	24.21	1.09	0.46
GUMA	150.865	−9.21	32.13	71.78	−1.04	16.25	1.81	1.81
HEHE	150.874	−10.226	34.27	58.86	1.6	3.34	1.29	0.95
*HOB2	147.439	−42.805	14.18	55.53	−0.43	−1.21	0.38	0.38
JONE	150.102	−10.095	34.82	59.22	1.95	3.4	0.7	0.92
KALO	150.43	−9.414	35.05	64.72	1.91	9.03	2.01	0.87
KAWA	150.299	−8.522	26.07	70.88	−7.51	15.14	1.48	1.24
KEIA	150.554	−10.213	34.67	58.27	1.94	2.62	1.52	1.03
KILI	150.292	−9.496	35.2	64.02	2.08	8.28	1.16	1.2
KIRI	172.923	1.355	−67.68	31.5	−105.81	−11.71	0.43	0.42
KURA	151.036	−10.11	34.44	57.44	1.74	1.98	1.8	0.69
KWAN	151.274	−9.923	33.48	59.48	0.73	4.11	1.16	0.68
KWAT	150.712	−9.311	32.1	71.31	−1.04	15.72	0.85	0.85
LELE	150.728	−10.302	33.82	55.94	1.16	0.36	0.8	1.47
LOS2	151.125	−8.535	24.86	71.13	−8.59	15.7	0.89	0.29
MAPA	150.437	−9.61	34.96	63.67	1.92	7.98	1.72	1.16
MENA	149.936	−9.757	35.49	62.81	2.44	6.93	0.27	1.58
*MOBS	144.975	−37.829	19.8	57.63	0.36	0.14	0.35	0.36
MORA	150.187	−9.432	32.48	66.08	−0.69	10.3	0.9	1.02
*NAUR	166.926	−0.552	−67.94	29.97	−104.75	−17.31	0.41	0.41
NUBE	149.867	−10.399	33.98	56.58	1.22	0.68	0.49	0.57
PEMM	149.795	−9.621	36.58	62.84	3.44	6.91	0.54	0.68
RABA	149.834	−9.972	35.83	62.48	2.86	6.57	0.57	0.85
SALM	150.796	−9.663	35.59	65.42	2.63	9.87	1.56	0.9
SIBA	150.268	−10.684	33.26	57.4	0.71	1.65	0.95	0.65
SIRI	149.708	−9.841	37.04	58.35	3.99	2.39	0.83	2.28
SMRI	150.662	−10.613	33	57.22	0.48	1.62	0.45	0.69
STRA	151.868	−10.225	35.09	59.33	2.59	4.2	0.85	0.48
*THTI	210.394	−17.577	−66.09	34.8	−83.7	25.59	0.39	0.39
*TIDB	148.98	−35.399	18.17	55.77	−0.45	−0.45	0.36	0.33
*TOW2	147.056	−19.269	28.91	56.67	−0.15	−0.2	0.43	0.46
TUF2	149.318	−9.079	31.11	64.4	−2.36	8.3	0.84	0.65
TUFI	149.323	−9.08	30.6	63.79	−2.87	7.69	1.64	1.13
*TUVA	179.197	−8.525	−64.19	32.52	−94.17	−5.92	0.43	0.51
UAMA	150.953	−9.452	33.7	71.71	0.66	16.22	1.72	1.64
VAKU	151.184	−8.853	29.55	74.3	−3.74	18.9	0.68	0.61
VIVI	150.324	−9.31	34.21	66.1	1.01	10.37	0.58	0.48
WAIB	150.139	−9.245	31.88	67.53	−1.38	11.73	0.85	0.7
WANI	149.157	−9.338	32.76	63.39	−0.61	7.23	0.9	0.68
WAPO	150.532	−9.355	33.51	69.43	0.36	13.78	1.72	2.1
WATL	150.243	−9.211	33.37	66.83	0.11	11.07	0.83	0.46
YANA	151.897	−9.271	33.37	75.61	0.39	20.49	1.16	1.08
*YAR2	115.347	−29.047	38.91	58.32	−0.55	0.35	0.33	0.51

[a]Sites with a * are continuous GPS sites with publicly available data on the Australian and Pacific Plates.

Miocene to Pliocene ages of metamorphic crystallization and exhumation in the UHP rocks are much younger than the Early Miocene cessation of Australian margin subduction after the Papuan arc-continent collision [*Little et al.*, 2011]. Models to explain the exhumation of the UHP rocks in SE PNG include: (1) a prolonged reversal of slip along a preexisting, shallowly dipping thrust contact between the Papuan Ultramafic Belt (PUB) and the UHP continental margin rocks [e.g., *Webb et al.*, 2008]; or (2) buoyancy-driven ascent of deeply subducted, partially molten continental fragments that rose nearly vertically as diapirs toward the

Table 2. List of Campaign GPS Sites and Years That We Have Observations for[a]

Site	1996	1997	2002	2004	2005	2006	2008	2009	2010	2011	2012
ALT2*			x	x				x	x		x
BASM								x	x		x
BAYA								x	x		x
BWAR								x	x	x	x
DAIO								x	x		x
DARB								x	x	x	x
DARW								x	x		x
DIGA								x	x		x
ESAA*				x			x		x		x
GIWA								x	x		x
GUA1*	X			x					x		
GUMA								x	x		x
HEHE								x	x		x
JONE								x	x		x
KALO								x	x		x
KAWA								x	x		x
KEIA								x	x		x
KILI								x	x		x
KURA								x	x		x
KWAN								x	x		x
KWAT								x	x		x
LELE								x	x		x
LOS2*		x		x					x		x
MAPA								x	x		x
MENA								x	x		x
MORA								x	x		x
NUBE								x	x		x
PEMM								x	x		x
RABA*				x		x	x	x			
SALM*				x			x		x		x
SIBA								x	x		x
SIRI								x	x		x
SMRI								x	x		x
STRA								x	x		x
TUF2								x	x		x
TUFI*				x	x	x					
UAMA								x	x		x
VAKU								x	x		x
VIVI*				x			x		x		x
WAIB								x	x		x
WANI								x	x		x
WAPO								x	x		x
WATL*				x			x		x		x
YANA								x	x		x

[a]Sites with a * are sites installed and observed prior to 2009 by Australian National University.

overlying thinned crust of the Woodlark Rift, ultimately to be emplaced into the upper crust of that rift as gneiss domes by 1.8–2.0 Ma [*Little et al*., 2011; *Ellis et al*., 2011; *Gordon et al*., 2012]. The latter model echoes the suggestion of *Martinez et al*. [2001] that the gneiss domes were emplaced in the crust via a diapiric, buoyancy-driven process. Today, the exhumed gneiss domes are flanked by active normal faults such as the Wakonai and Mwadeia faults. These are clearly active structures as indicated by the dramatic alignment of faceted spurs along their scarps, and other geomorphic evidence [*Hill*, 1994; *Little et al*., 2007, 2011; *Miller et al*., 2012]. *P* wave tomography studies show a large, low velocity region beneath the D'Entrecasteaux Islands, interpreted as significant thinning of the lithosphere, leading *Abers et al*. [2002] to suggest that mantle buoyancy provides isostatic support for the high elevations in the D'Entrecasteaux Islands.

3. Data Used in This Study

3.1. GPS Data Acquisition and Processing

To determine the distribution of crustal strain related to continental rifting and UHP rock exhumation, we installed and measured a campaign GPS network of ~40 sites throughout southeastern PNG in 2009, and remeasured the sites in 2010 and 2012 (Figure 2, Table 1). Papua New Guinea is rugged and remote, so we focused our efforts on coastal sites that we could access by boat. Prior to 2009, Australian National University (ANU) had undertaken campaigns measuring at several other sites in southeastern PNG (ALT2, RABA, VIVI, WATL, ESAA, SALM, LOS2; TUFI; GUA1); we remeasured most of these sites during 2009–2012, and included these earlier ANU data in our analysis. TUFI was destroyed sometime between 2006 and 2009, so we replaced that site with a new one (named TUF2). All data during the 2009–2012 campaigns were collected using Trimble 5700 or Trimble R7 receivers and Zephyr geodetic antennas. Table 2 contains a list of the GPS sites, and the years for which we have data. For the 2009–2012 campaigns we obtained at least 2 (typically more) 24 h sessions at each site during each campaign.

We processed the GPS data using GAMIT/GLOBK software [*Herring et al*., 2010a, 2010b]. The procedure used in this type of analysis has been reviewed extensively in *Feigl et al*. [1993], *Herring et al*. [1990], *McClusky et al*. [2000], and *Tregoning and Watson* [2009, 2011]. For the first stage of the processing, we estimate station coordinates of a regional network, the zenith delay of the atmosphere at each station, and orbital and earth orientation parameters (EOP's) using doubly differenced GPS phase observations. All of these parameters are loosely constrained in this step. We also account for ocean tidal loading (from Onsala Space Observatory, http://froste.oso.chalmers.se/loading/) and atmospheric loading (nontidal plus S1 and S2 tidal effects

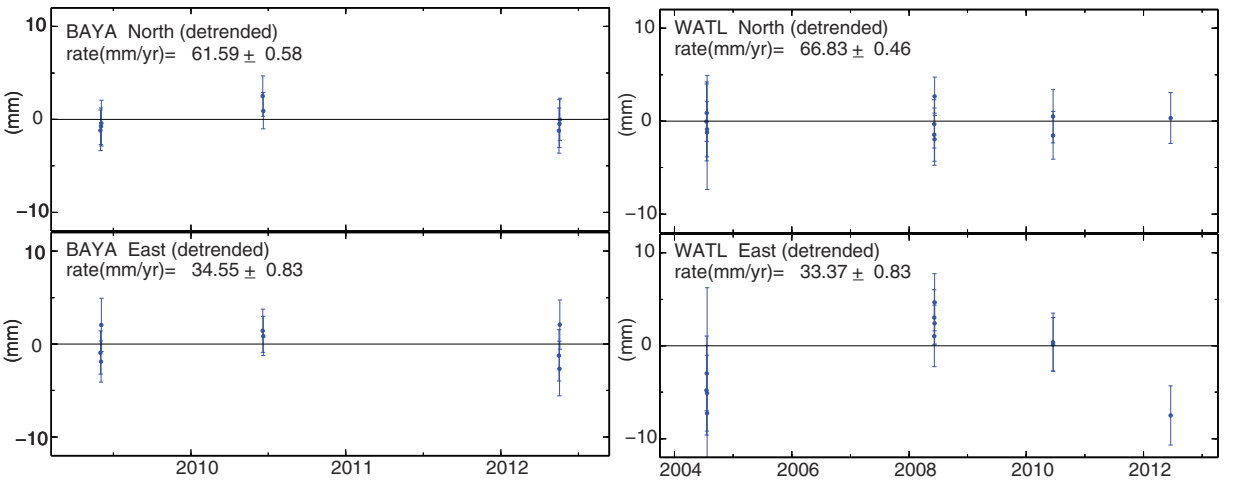

Figure 3. Example time series of GPS observations from two representative sites.

[*Tregoning and Watson*, 2009]) in the processing. We use Vienna Mapping Function (VMF1) in our determination of atmospheric delay [*Boehm et al.*, 2006]. In the processing, we also included GPS data from several long-running International GPS Service (IGS) sites in the Australia/Pacific region, in order to link our network with the IGS network of sites.

To calculate site positions and velocities in a consistent reference frame (ITRF2008) [*Altamimi et al.*, 2011], we use our solutions (EOP's, orbital parameters, and coordinates and their covariances) from GAMIT, and solutions (performed by MIT, as part of their processing for the International GNSS Service) of the global IGS network. These solutions are combined using GLOBK (a Kalman filter) [*Herring et al.*, 2010b]. To align our network with ITRF2008, we place tight constraints on the ITRF2008 velocities of 46 core IGS sites and estimate a rotation and translation to align our solutions with ITRF2008. Table 1 shows our PNG site velocities (and a subset of Pacific and Australian Plate sites) in both ITRF2008 and Australian Plate-fixed reference

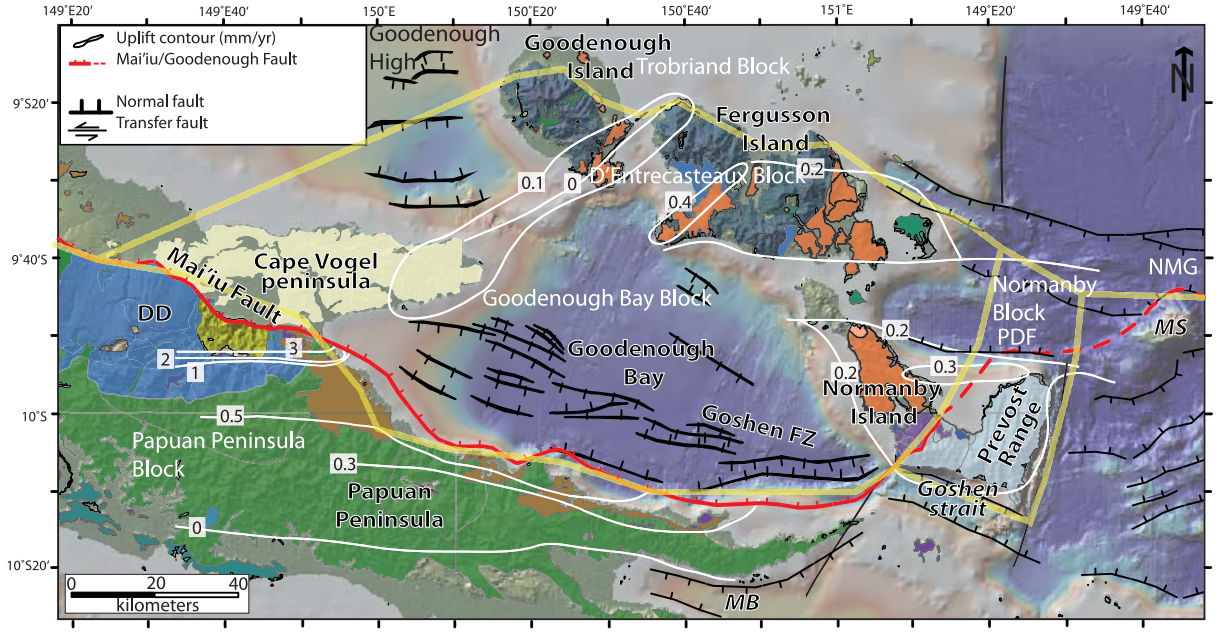

Figure 4. Detailed setting of the continental portion of the rift overlain with our preferred block model geometry. White contours show uplift rates from *Fitz and Mann* [2013a, 2013b]. Figure modified from *Fitz and Mann* [2013a]. PDF = Prevost Detachment Fault; MS = Moresby Seamount; MB = Milne Bay; DD = Dayman Dome; NMG = North Moresby Graben.

frames, with uncertainties estimated from the time series. Errors in campaign GPS site velocities are often underestimated [*Mao et al*., 1999], due to various sources of unmodeled noise. To account for this, we multiply all our formal errors (output by GLOBK) by a factor of 1.5. To calculate the velocities relative to Australia, we solve for a rotation of the data set (e.g., an angular velocity describing rotation of our realization of ITRF08 relative to the Australian Plate) that minimizes the velocities at Australian Plate sites (Table 1). Time series of a few representative examples of the PNG campaign GPS sites are shown in Figure 3.

It is possible that some of the Australian National University campaign sites that underwent observations prior to 2009 (LOS2, GUA1, ALT2, ESAA, SALM, RABA, VIVI, and WATL) were displaced coseismically by (a) the 16 November 2000 Mw 8.0 New Ireland, Papua New Guinea earthquake, 500–800 km from our GPS network, and (b) 1 April 2007 Mw 8.1 Solomon Islands earthquake, on the San Cristobal and New Britain Trenches 500–900 km from our network [e.g., *Taylor et al*., 2008a, 2008b; *Furlong et al*., 2009]. The GPS site time series at these sites are not temporally dense enough to reliably estimate and remove the coseismic offset from either the 2000 or the 2007 earthquake, if there was any. To assess possible coseismic displacements of the earlier campaign sites due to the large, distant earthquakes, we use calculations for our sites from *Tregoning et al*. [2013] (see also for the Great earthquake calculator online: http://rses.anu.edu.au/geodynamics/Great_earthquake_deformation/). *Tregoning et al*. [2013] model estimates of static co-seismic deformation in global great earthquakes since 2000, using a spherical layered model [*Pollitz*, 1996]. Surface deformation is calculated assuming the PREM elastic stratification [*Dziewonski and Anderson*, 1981], with a spherical harmonic expansion from degrees 1 to 1500. From these calculations at each of the pre-2009 campaign sites, we find that the impact of the 2007 Solomon Islands on most of the pre-2009 campaign GPS sites is negligible ($<$a few mm total displacement), with the exception of GUA1 and LOS2, which are the sites closest to the 2007 earthquake. LOS2 and GUA1 are also the only sites where we use pre-2000 data, so we correct for both the 2007 and the 2000 earthquake in our estimation of the velocities at those two sites. For the 2007 earthquake, the magnitude of the correction of GUA1 is $\sim$8.7 cm, while the correction at LOS2 (which is further from the earthquake) decreases to $\sim$1.6 cm. For the 2000 earthquake, we correct GUA1 and LOS2 by $\sim$1.3 cm.

4. Interpretation of the GPS Results

Overall, the GPS results from sites in the Trobriand Islands (KAWA, LOS2, VAKU), Woodlark Island (GUA1), Egum Atoll (YANA), and Cape Nelson (TUFI, TUF1, WANI) are consistent with anticlockwise rotation of the microplate north of the Woodlark Basin (Figures 1 and 2), as suggested by previous studies [*Tregoning et al*., 1998; *Wallace et al*., 2004]. The small vectors at sites on the Papuan Peninsula mainland suggest that the Papuan Peninsula has motion similar to the Australian Plate, while the fast northward motion ($>$10 mm/yr) of sites in the D'Entrecasteaux Islands suggest a large amount of extensional deformation is being accommodated within Goodenough Bay. Relatively slow velocities of sites on Normanby Island suggest that most of the extensional deformation in that area (east of 150.75°E) is being accommodated offshore to the north of Normanby Island, in the Dawson Strait, and further east in the area of the Moresby Seamount, where there is a well-expressed $\sim$30° dipping fault that has accommodated $\sim$8 km of normal-slip since the Pliocene [*Taylor and Huchon*, 2002; *Speckbacher et al*., 2011]. This fault also coincides with the majority of magnitude 5 and larger earthquakes in the region, indicating that it is significantly active [*Abers et al*., 1997].

To jointly interpret the GPS velocities and additional kinematic data (transform orientations and earthquake slip vectors), we use an elastic block modeling program, DEFNODE, developed by *McCaffrey* [2002]. This approach allows us to invert GPS velocities, active fault slip rates and slip azimuths, and earthquake slip vectors for poles of rotation of elastic crustal blocks and the degree of interseismic coupling on faults bounding the crustal blocks. Such an approach is important to use in a place like southeastern PNG, where the GPS velocity field is strongly influenced by rapid block rotations [*Tregoning et al*., 1998; *Wallace et al*., 2004], as well as possible elastic strain related to interseismic coupling on faults in the region. DEFNODE applies simulated annealing to downhill simplex minimization [e.g., *Press et al*., 1989] to solve for the angular velocities of the specified tectonic blocks and coupling coefficients for faults between the blocks. We minimize data misfit, defined by the reduced chi-squared statistic (χ^2_n). The method also allows us to optimally rotate multiple GPS velocity solutions into a common reference frame.

The short-term (interseismic) slip rate within a few tens of kilometers of most faults is considerably less than the long-term slip rate expected from the relative motion of the adjacent tectonic blocks. This slowing is

due to elastic strain buildup within the crust adjacent to the fault caused by the friction (sometimes called "locking" or "coupling") between the two sides of the fault. For our purposes, we refer to a purely kinematic quantity we call the "coupling coefficient," ϕ, to describe the process whereby friction causes the fault to be stuck for long periods. If $\phi = 0$, the fault is creeping at the full long-term slip rate and if $\phi = 1$ there is no creep in the interseismic period (i.e., the fault undergoes complete interseismic locking). The relative motion (slip) vector on the faults ($\boldsymbol{V}$) is determined by the Euler vectors describing the motions of the blocks on either side of the fault. The slip rate deficit vector on the fault is the scalar coupling value ϕ multiplied by the relative motion vector V between the two blocks at a given fault point. The elastic contribution to the velocity field from the fault slip rate deficit is calculated using a back-slip approach to elastic dislocation modeling [*Savage*, 1983], using the formulations of *Okada* [1985] for surface displacements due to dislocations in an elastic half-space.

We divide southeastern PNG into multiple tectonic blocks based on the locations of known, active faults (Figures 1 and 4). However, we note that large portions of the blocks we show in Figure 4 are submerged beneath the sea (such as the Goodenough Bay Block), and the independence and detailed kinematics of some of these blocks is impossible to determine with the land-based GPS on its own (see section 4.3). One of the primary fault systems that we use as a block boundary is the Mai'iu Fault, which most researchers suggest is the primary plate boundary fault in the region [e.g., *Fitz and Mann*, 2013a; *Little et al*., 2007; *Spencer*, 2010; *Dazcko et al*., 2011]. We also use active normal faults identified on the northern flanks of Goodenough and Fergusson Islands, as well as likely active features on the south coast of Fergusson [*Little et al*., 2007]; the Goshen Strait Fault zone south of Normanby Island [*Mutter et al*., 1996; *Little et al*., 2007; *Fitz and Mann*, 2013a]; a transfer structure cross-cutting Normanby Island [*Little et al*., 2007]; and a transfer fault on the east flank of Normanby Island [*Benes et al*., 1994; *Little et al*., 2007]. Seismic reflection data show significant active extensional deformation observed on normal faults within Goodenough Bay on the Goshen Fault Zone [*Mutter et al*., 1996; *Fitz and Mann*, 2013a] (Figure 4), and therefore internal deformation of our Goodenough Bay Block is likely. However, there are no GPS sites within Goodenough Bay, so it is not possible to determine the partitioning of deformation among the faults of the Goshen Fault Zone. Slip rates that we obtain for the southern boundary of the Goodenough Bay Block are total slip rates representative of the entire zone of faults within Goodenough Bay. We also note that if the normal faults on the north flank of the D'Entrecasteaux Islands accommodate significant extensional deformation, a kinematic issue arises in terms of transferring that deformation to the Mai'iu Fault in the Papuan Peninsula further west, which appears to be the primary feature accommodating plate motion west of 150°E. There is no evidence for substantial active extension within the Trobriand Platform north of ~9°S [*Fitz and Mann*, 2013a]. We suggest that normal faults such as those that have been mapped west of Goodenough Island and North of Cape Vogel (Figure 4) [*Fitz and Mann*, 2013a, 2013b] help to accommodate this westward transfer of deformation to the Mai'iu Fault, and we include a boundary between the Goodenough Bay Block and the Trobriand Block here. A regional seismicity study by *Dieck et al*. [2013] also reveals a distinct zone of shallow microseismicity coinciding with this boundary projecting from Cape Vogel to Goodenough Island. Their shallow seismicity distribution also follows the dome-bounding faults, and agrees well with the boundaries we have defined for the D'Entrecasteaux Islands Block. In section 4.3, we will test for independence of these crustal blocks. For the faults in our block model (Figure 4), we solve for coupling coefficients at nodes on the fault. In most cases, we treat several adjacent fault nodes as a single parameter. Thus, for all of the faults in our southeast PNG model, free parameters for interseismic coupling are typically reduced to 1–3 for each fault, depending on the length of the fault.

We also acknowledge that due to the diffuse nature of much of the extensional deformation observed in the continental portion of the Woodlark Rift (Figures 1 and 4) a tectonic block approach is certainly not a perfect way of interpreting the GPS velocities. Rather, we employ this approach to (1) place some constraints on where, and at what rates, the bulk of the extensional deformation occurs, (2) to understand the kinematics of how deformation is transferred from the seafloor spreading area to the continental rifting region, and (3) to better constrain the kinematics of crustal block rotations across the Woodlark Basin region.

4.1. Additional Kinematic Data Used

In addition to the GPS velocities, we also use kinematic data such as earthquake slip vectors and transform fault orientations. The earthquake slip vector and transform orientation data give us information about the

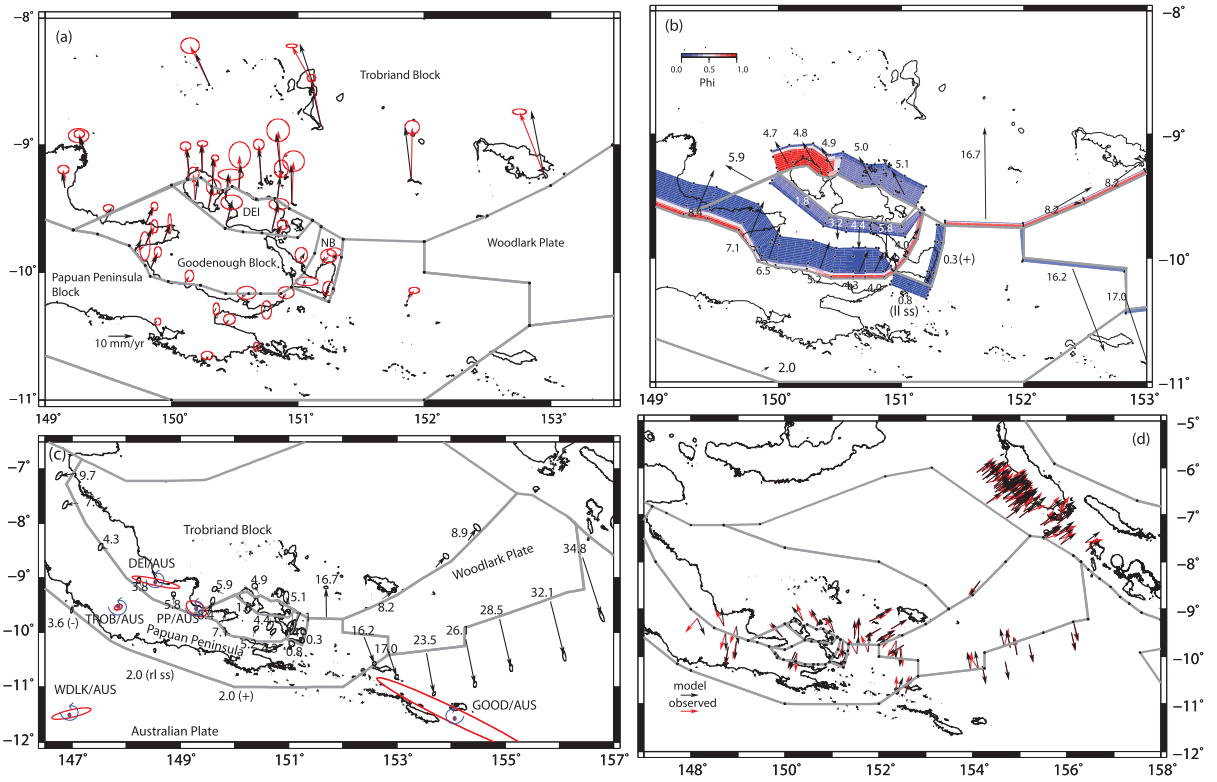

Figure 5. Results from our preferred block model. (a) Fits to the GPS data (red = observed, black = model). Uncertainty ellipses 95% confidence; (b) fault slip rates and locking results shown in terms of coupling coefficient (Phi), where 0 = creeping and 1.0 = fully locked; (c) fault slip rates for the broader region with poles of rotation for the blocks relative to Australia. Rates (mm/yr) with black vectors show relative motion between adjacent blocks. In general, the motion shown at the block boundaries is for the hanging wall block relative to the footwall block (see Figure 5b for the fault geometries). (d) Earthquake and transform slip vector results (red = observed, black = model). D'Entrecasteaux Islands = DEI.

relative motion between the blocks, and help to constrain poles of rotation. For the earthquake slip vectors, we use earthquakes from *Abers et al*. [1997], as well as shallow earthquakes from the Global CMT project [*Dziewonski et al*., 1981; *Ekstrom et al*., 2012]. We only use shallow earthquakes (<35 km deep) from both of these data sets. For the slip vector calculations, we use the focal planes that are consistent with known active faults in the area. We assume uncertainties of 20° for the earthquake slip vectors. The transform orientations are from the latest phase of rifting (e.g., the last 80 kyr) from *Goodliffe et al*. [1997]. Figure 5d shows the slip vector and transform fault directions used in our study (red arrows). The transform and slip vector orientations are particularly useful to help constrain the motion of the Woodlark Plate, which does not contain any GPS sites.

4.2. Preferred Elastic Block Model Results

Our preferred block model consists of six crustal blocks (in addition to the Australian and Pacific Plates): the Woodlark Plate, the Trobriand Block, the Goodenough Bay Block, the Papuan Peninsula Block, the D'Entrecasteaux Block, and the Normanby Block (Figure 5). We also invert for locking on faults bounding these structures (Figure 5b). The $\chi^2_n = 1.39$ in our best fitting model. The Woodlark, Trobriand, D'Entrecasteaux, and Normanby blocks are rotating anticlockwise at a rapid rate (~2–3°/Myr) (Figure 5c and Table 3). The poles of rotation are located near the western termination of the rift (Figure 5c). In contrast, the Goodenough Bay Block appears to be rotating in a clockwise fashion (at ~0.9°/Myr) about a pole east of the rift (Figure 5c and Table 3), producing an eastward decrease in slip rates on the Mai'iu Fault north of the Papuan Peninsula. This eastward decrease in slip rates is consistent with the observation of eastward decreasing coastal uplift rates in the footwall of the fault [*Fitz and Mann*, 2013b] (Figure 4, white contours), and with the more subdued topographic expression and decreased relief of the fault scarp in that direction [*Spencer*, 2010].

Overall, our best fitting model is consistent with the idea that the rates of rifting are highest in the eastern Woodlark Basin (up to 34.8 ± 3 mm/yr), and decrease westward to 17 ± 1 mm/yr near 152°E, and

Table 3. Poles of Rotation for the Tectonic Blocks Relative to the Australian Plate

Plate Pairs	Longitude	Latitude	Rotation Rate (°/Myr)	Major Axis Uncertainty (Distance in Degrees)	Minor Axis Uncertainty (Distance in Degrees)	Orientation of Major Axis (in ° East of North)
AUST/WDLK	146.99	−11.48	1.85 ± 0.29	1.25	0.24	77
AUST/TROB	147.85	−9.54	2.69 ± 0.13	0.26	0.15	64
AUST/DEI	148.55	−9.08	2.49 ± 1.46	1.52	0.2	282
AUST/GOOD	154.09	−11.54	−0.87 ± 0.77	5.47	0.46	116
AUST/NORM	150.52	−9.75	1.73 ± 0.44	0.61	0.31	84
AUST/PP	149.29	−9.57	0.66 ± 0.15	0.7	0.4	301

Cartesian Poles, Uncertainties, and Covariances

Plate Pairs	Ω_x	Ω_y	Ω_z	σ_x	σ_y	σ_z	cov(x,y)	cov(x,z)	cov(y,z)
AUST/WDLK	−1.52	0.99	−0.37	0.26	0.13	0.05	−0.0348	0.0135	−0.007
AUST/TROB	−2.24	1.41	−0.45	0.11	0.06	0.02	−0.0065	0.002	−0.0011
AUST/DEI	−2.10	1.28	−0.39	1.25	0.71	0.24	−0.8952	0.3012	−0.1716
AUST/GOOD	0.77	−0.37	0.17	0.66	0.38	0.13	−0.2473	0.084	−0.0483
AUST/NORM	−1.49	0.84	−0.29	0.38	0.20	0.07	−0.0776	0.0272	−0.0145
AUST/PP	−0.56	0.33	−0.11	0.13	0.07	0.03	−0.0097	0.0037	−0.002

8.4 ± 1.2 mm/yr near 149.5°E (Figure 5c). Further north along the Owen Stanley Fault Zone (Figure 1), the relative motion becomes left-lateral strike slip, and then gradually rotates around to east-west contraction north of 8.5°S at rates of ∼1 cm/yr (Figure 5c). Although we do not have GPS sites on the Woodlark Plate itself, the contemporary rates of Woodlark-Australia seafloor spreading are reasonably well constrained by the overall total extension budget imposed by the motion of the Trobriand Block relative to Australia, as well as information from the earthquake slip vectors and transform orientations from faults on the boundaries of the Woodlark Plate. The slip vectors and transforms help to inform the direction of motion of the Woodlark Plate relative to its better-constrained neighbors (Figure 5d). For the Nubara Fault (Figure 1), we estimate a right-lateral slip rate of 8–9 mm/yr, largely constrained by the plate motion budget imposed by the Trobriand Block in addition to the kinematic constraints from earthquake slip vectors. In the continental portion of the rift, and particularly in the region of UHP rock exhumation in the D'Entrecasteaux Islands, deformation is more complex and broadly distributed, with total rates of rifting on the order of 13–16 mm/yr. In our best fitting block model results, between 150°E and 151°E, nearly equal portions of the plate motion are partitioned between structures surrounding the D'Entrecasteaux Islands and Mai'iu Fault (e.g., 4–7 mm/yr on each system; Figure 5c). In our best fitting model, we estimate 4 ± 2 mm/yr of right-lateral strike slip on the transfer structure inferred to cross-cut Normanby Island [e.g., *Little et al*., 2007]. However, we note that while Little et al. suggested at least some finite left-lateral slip on this structure, our results require contemporary right-lateral slip. Structures east and south of Normanby appear to have low rates of activity (<1 mm/yr) in the best fitting model.

We treat the Papuan Peninsula and some of the islands south of the Woodlark Basin as a single block (the Papuan Peninsula Block). We have only one GPS site south of the spreading center (STRA), so the eastward extent of this block (beyond STRA) cannot be defined with existing data. However, the sites on the Papuan Peninsula and STRA can be fit well with a single pole of rotation. Slow northward motion (∼1–2 mm/yr) of the GPS sites on the Papuan Peninsula (Figures 2 and 5) suggest that there may some ongoing, slow extension (<1–2 mm/yr) between the Papuan Peninsula and Australia, possibly occurring in the Aure Trough (Figure 1). More rapid northward motion of GPS site STRA (Figure 2) suggests that up to ∼4 mm/yr of extension may be distributed across the Pocklington Rise and Graben to the south of the Woodlark Spreading Center, at least in the region of 152°E. To the west, our Papuan Peninsula/Australia pole suggests slow (less than a few mm/yr) contraction between Australia and the Papuan Peninsula (west of 148°E), which we suggest may also be accommodated in the Aure Trough south of PNG. To better constrain the style and rate of possible slow deformation between the southern PNG and Australia, installation of additional GPS sites throughout the Papuan Peninsula and Pocklington Rise area is needed.

Based on their low interseismic coupling coefficients, the majority of the faults in our best fitting model appear to be mostly aseismically creeping (Figure 5b), with the possible exceptions of the shallowest portion of the Mai'iu Fault, and the fault flanking the northern side of Goodenough Island, although we note that locking on many of these structures is not well constrained due to the configuration of the GPS network. Given that the faults in our best fitting inversions appear to be mostly aseismically creeping, we also

Table 4. Results of F Tests to Distinguish Between the Different Models[a]

Model	N_{data}	$N_{parameters}$	DOF	χ^2_n
(1) Best fit	274	35	239	1.39
(2) Rotation only (no locking)	274	21	253	1.63
(3) GOOD + DEI + TROB	270	29	241	2.25
(4) DEI + GOOD, strain	274	35	239	1.49
(5) NORM + GOOD	274	31	243	1.41
(6) NORM + GOOD + DEI, strain	274	32	242	1.62
(7) DEI + TROB	274	30	244	1.51
Comparison of Models	*F* Test Probability			Inference
Is (1) better than (2)?	0.89			Probably
Is (1) better than (3)?	0.99			Yes
Is (1) better than (4)?	0.70			Probably
Is (1) better than (5)?	0.54			No
Is (1) better than (6)?	0.88			Probably
Is (1) better than (7)?	0.74			Probably

[a]GOOD = Goodenough Bay Block; DEI = D'Entrecasteaux Block; TROB = Trobriand Block; NORM = Normanby Block. GOOD + DEI + TROB means that we have combined those blocks together. Where we say "strain" in the model description, we have estimated the three components of the horizontal strain tensor to enable uniform strain of the composite block (approximating distributed deformation within the block).

run an inversion with no fault locking at all (inverting for poles of rotation only), and obtain a $\chi^2_n = 1.63$ (compare to our preferred model with some fault locking that has a $\chi^2_n = 1.39$). The similarity in fit to the data for models with fault locking versus those without fault locking suggests that the GPS data do not require a large amount of elastic strain due to interseismic coupling on faults in the region to produce a statistically significant improvement in fit to the data (see also Table 4). This result implies that: (1) faults in the continental portion of the rift are dominated by aseismic creep, and/or (2) that the current network configuration is not well suited to capturing interseismic fault coupling. The historical rates of seismicity in the Woodlark rift are low, much less than that expected from the overall plate motion budget [*Abers et al*., 1997], which is compatible with the possibility that most of the overall plate boundary deformation in the continental portion of the rift is accommodated aseismically. This result suggests that seismic hazard in the southeast PNG region may be lower than expected based on the total relative plate motion that occurs there. However, a denser GPS network is needed to confirm this.

We treat the Solomon Sea Plate as part of the Trobriand Block in our preferred model (and all other models presented here), under the assumption that the Trobriand Trough is no longer active. However, we cannot test whether or not this is true as there are no GPS sites on the Solomon Sea Plate (it is submarine). Furthermore, there are not enough historical earthquakes on the Trobriand Trough structure (Figure 1) to help constrain the sense of relative motion between the Trobriand Block and a separate Solomon Sea Plate, if indeed they are separate tectonic plates. In section 5.4, we discuss other lines of evidence suggesting that the Trobriand Trough no longer accommodates active subduction.

4.3. Tests for Block Independence

To quantify the uniqueness of our results, and to what degree we have confidence in our fault slip rate estimates and microplate kinematics for the southeast PNG region, we have conducted additional block model inversions using a suite of alternative configurations (Table 4; results from some examples are shown in Figure 6) to compare the results with our preferred model. In general, we have tried scenarios that combine different tectonic blocks into single, composite blocks to test if they are independent from each other, hence allowing us to test if the GPS data require particular fault systems to be active. In some cases, we can confidently rule out particular scenarios—for example, the scenario where the Trobriand Block, Goodenough Bay, and D'Entrecasteaux blocks are part of a single composite block—we can say at 99% confidence that this scenario is not valid. This result confirms that the GPS data require deformation on faults within and surrounding the D'Entrecasteaux Islands, and that the Mai'iu Fault is not the only active fault system in the continental portion of the rift. Other models, such as the one where we combine the D'Entrecasteaux and Goodenough Bay blocks (Figure 6a), and allow internal strain of those blocks produce a poorer fit ($\chi^2_n = 1.62$) than our best fitting model ($\chi^2_n = 1.39$); when we conduct an *F* test there is an 88% chance that separating the Goodenough Bay and D'Entrecasteaux blocks produces an improved fit to the data. Based on the *F* test results, one of the scenarios that we are the least certain about is if the Normanby and Goodenough Bay blocks are two separate blocks—there is only a 54% chance that they are separate. This has implications for whether or not the transfer structure cutting through Normanby Island [*Little et al*., 2007] is active or not. In the case, where the Normanby and Goodenough Bay blocks are a single block (Figure 6b), this requires dextral strike slip to occur on the north-south trending structure to the east of Normanby Island, together with increased extension rates on the Goshen Strait Fault Zone to the south of Normanby

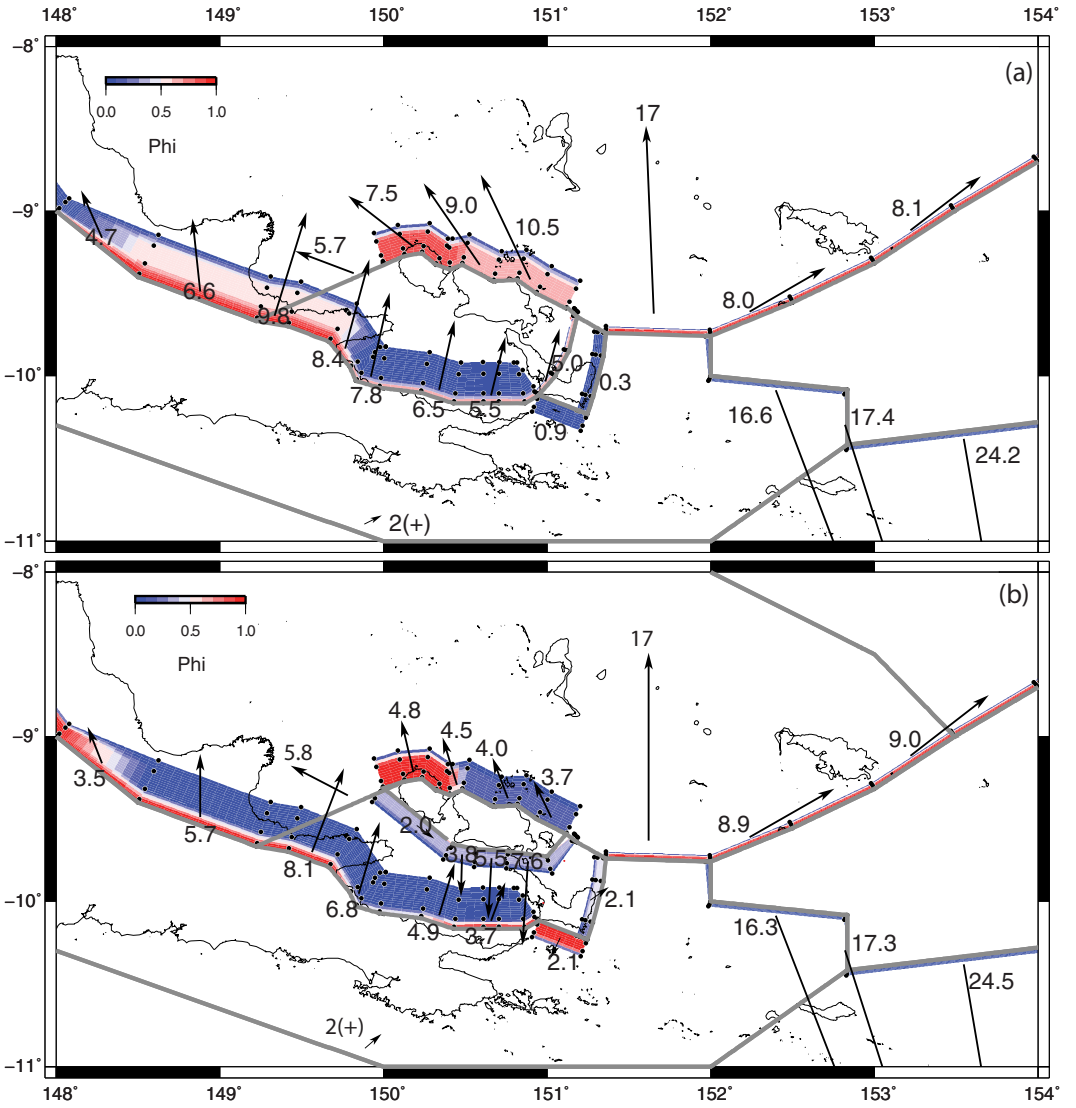

Figure 6. Fault locking and slip rate results from two of the alternative block model configurations (a) the model where the Goodenough Bay and D'Entrecasteaux Blocks are a single composite block, and (b) a model where the Goodenough Bay and Normanby blocks are a single composite block.

Island (both boundaries must slip at ∼4 mm/yr). Thus, it is difficult to determine with great confidence the slip rates on any of the structures bounding the Normanby Block using GPS data alone—rates could range from less than 1 mm/yr up to 3 mm/yr. As we discussed in the previous section, when we run models using the preferred block configuration, but with no locked faults in them (e.g., no elastic strain) we obtain an equivalent fit to the GPS data (compare models 1 and 2 in Table 4).

5. Discussion

5.1. Continental Rifting and Partitioning of Extensional Deformation Across SE PNG

Our GPS results indicate that continental rifting in the region of the D'Entrecasteaux Islands and Goodenough Bay is distributed over an ∼100 km wide region (Figure 5). This is in contrast to the area north and east of Normanby Island, where the majority of the plate motion is accommodated in a narrow corridor that includes the Prevost Detachment fault [*Little et al.*, 2007; *Miller et al.*, 2012] and, farther to the NE, the active faults bounding Moresby Seamount [*Taylor and Huchon*, 2002; *Goodliffe and Taylor*, 2007; *Speckbacher et al.*, 2011]. Deformation localizes to a greater extent east of ∼151.5°E where seafloor spreading occurs [*Taylor*

et al., 1999]. Our results show that at least half of the overall continental rifting budget is accommodated on faults that bound the gneiss domes of the D'Entrecasteaux Islands (Figure 5). The remainder of the overall plate motion budget is transferred southward from the seafloor spreading center and the Moresby Seamount/Prevost Detachment faults into the southern half of Goodenough Bay, including onto the Goshen Fault Zone offshore and the Mai'iu Fault along the NE margin of the Papuan Peninsula [e.g., *Little et al*., 2007; *Fitz and Mann*, 2013a]. Right-lateral transfer structures, such as that inferred to cross-cut Normanby Island are critical to accomplish this southward transfer and broadening of rift-related deformation as it propagates into the continent. Clockwise rotation of the Goodenough Bay Block may also be a consequence of the southward transfer of deformation from the spreading center to the Mai'iu Fault. Clockwise rotation of the Goodenough Bay Block about a pole southeast of the Papuan Peninsula (Figure 5) requires a westward increase in slip rate on the Mai'iu Fault, enabling transfer of much of the plate motion budget onto that fault system. A westward increase in slip rate on the Mai'iu Fault agrees well with a westward increase in Holocene coastal uplift rates on the south side of Goodenough Bay, adjacent to the fault (Figure 4) [*Fitz and Mann*, 2013b]. Together with this clockwise rotation of the Goodenough Bay Block and westward increase in Mai'iu fault slip rate, there is a corresponding westward decrease in the amount of extension accommodated on the south side of the D'Entrecasteaux Islands. Thus, clockwise rotation of the Goodenough Bay Block accompanies (and facilitates) eventual localization of most of the plate motion budget onto the western Mai'iu Fault, a structure that bounds the rapidly exhuming Dayman Dome metamorphic core complex (Figures 4 and 5). This is similar to a conceptual model for partitioning of extensional deformation in the Aegean region developed by *Goldsworthy et al*. [2002]. They proposed that clockwise rotation of the tectonic block located between the Gulf of Evia and the Gulf of Corinth is produced by a westward decrease of rifting rates in the Gulf of Evia (analogous to rifting in the D'Entrecasteaux Islands), and a concomitant westward increase in rifting rates in the Gulf of Corinth (analogous to the Mai'iu Fault).

Total rates of north-south extension across the rift from GPS vary from 17 mm/yr near 151.5°E, decreasing to ~13 mm/yr near 150°E. *Fitz and Mann* [2013a] and *Kington and Goodliffe* [2008] conducted structural reconstructions of north-south oriented seismic profiles across the rift (see Figure 1, for profile locations) to determine finite upper crustal extensions in the region over the last 8.4 million years and compared these with estimates of middle/lower crustal extension from subsidence data along the profiles. *Kington and Goodliffe* [2008] obtained brittle extension estimates of ~111 km along a transect crossing the Moresby Seamount (see Figure 1, for transect locations), while the subsidence data similarly predicts 115 km of extension. At the current GPS extension rates of 17 mm/yr for that portion of the rift (Figure 5), it would take 6.5–6.8 Myr to accommodate this amount of extension, similar to the postulated age of the onset of rifting in the SE PNG region between 8.4 and 6 Ma [*Taylor and Huchon*, 2002]. Although 111–115 km of extension is ~50% lower than that expected from Woodlark-Australia Euler Poles derived from seafloor spreading data in the Woodlark Spreading Center, the Woodlark-Australia Euler poles are not necessarily representative of plate motions in the continental portion of the rift, where tectonic blocks with different kinematics may be involved [e.g., *Kington and Goodliffe*, 2008]. Extension in the Moresby Seamount area reflects relative motion between the Trobriand Block and the Australian Plate, not Woodlark Plate/Australia relative motion.

Further west, *Fitz and Mann* [2013a] obtain larger discrepancies in extension rates from brittle extension, subsidence data, and our GPS-derived rates. In their Profile 1 (Figure 1), they estimate 2.3 km of upper crustal extension (from brittle faulting) compared to 20.7 km for the mid/lower crust (from subsidence data). Profile 2 yields estimates of 13.4 and 23.1 km for upper crustal and lower crustal extension (respectively), while Profile 3 suggests 6.3 km upper crustal and 23.6 km of lower crustal extension. Such discrepancies in upper versus lower crustal extension estimates [see also *Kington and Goodliffe*, 2008] led *Little et al*. [2007] and *Fitz and Mann* [2013a] to conclude that the lower crust is weak and has flowed outward from beneath the mountainous rift margins to advance beneath the Woodlark Rift into the Trobriand Platform and Goodenough Basin, and beneath the D'Entrecasteaux Islands, with this lower crustal material eventually being exhumed to the surface in the gneiss domes of the D'Entrecasteaux Islands. We compare the total extension estimates of *Fitz and Mann* [2013a] over the last 8.4 Myr with our contemporary rates in the region of the Profiles 2 and 3 by taking the upper crustal extension values and then adding to that the width of the D'Entrecasteaux Islands gneiss domes (34 km on profile 2, and 32 km on Profile 3) that have intruded into the upper crust there. The total upper crustal extension (since 8.4 Myr) estimated in this way on Profiles 2 and 3 is 47.4 km and 38.3 km, respectively. Using the total north-south extension rates

determined from GPS along these profiles (12 mm/yr on profiles 2 and 3), it would take 3.2–4.0 million years to accommodate these magnitudes of total upper crustal extension on these profiles at modern-day rates. That all of this extension may have occurred in the last 3–4 million years is consistent with the ~2.4 Ma age of final ductile deformation on the Mailolo Dome on Fergusson Island, and the 1.8–2.0 Ma timing of final emplacement of that gneiss dome into the upper crust [see *Little et al*., 2011; *Gordon et al*., 2012]. If the crustal extension was instead distributed over a longer time interval extending as far back as 8.4 Ma, then it would indicate a mean extension rate of 4.6–5.6 mm/yr; which is three times slower than our measured modern-day rate.

There are three options to explain the difference in extension rates determined from GPS and geological methods [*Fitz and Mann*, 2013a]: (1) the extension rates in the Goodenough Bay and D'Entrecasteaux Islands region were much lower in the past, and have only recently increased to their current fast rates in those locations in the last few Myr; (2) that the total extension that has occurred in the southeastern PNG region, especially prior to ~3 Ma, has been under-estimated geologically; or (3) some combination of both scenarios. Normal faults have been imaged further to the south of Goodenough Bay, in the Milne Bay Graben and in the Pocklington Basin, although little is known about the timing and magnitude of extension accommodated by these features. It is possible that some portion of the current GPS extension budget was accommodated on these more southerly features earlier in the rifting history (Option 2), and that deformation has become progressively localized northward into the Goodenough Bay and D'Entrecasteaux Islands regions as rifting has progressed. Recent paleomagnetic data [*Cairns et al*., 2013] supports this model—with data recording an anticlockwise rotation of Miocene rocks on the southern side of the SE Papuan Peninsula relative to the Australian Plate, requiring extensional deformation south of the Papuan Peninsula since the Miocene. However, we also note that *Fitz and Mann* [2013a] reconstruct ~3–4 km of extension on the Mai'iu Fault (referred to as the Owen Stanley Fault in that paper), largely based on seismic reflection data from the hanging wall that does not extend far enough south to image the fault itself or the footwall. This fault is probably developing via a rolling-hinge mechanism [*Spencer*, 2010], so reconstructions based purely on the magnitude of hanging wall subsidence will severely underestimate the total extension accommodated by the fault [e.g., *Lavier and Manatschal*, 2006]. The exhumed width of the scarp on the footwall suggests >20 km of additional extension. Moreover, *Reston* [2007] demonstrates that magnitudes of upper crustal extension observed at many rifted margins may be severely underestimated due to unrecognized polyphase faulting and flexural rotation of slip surfaces to follow the top of the basement. Thus, upper crustal extension rates in *Fitz and Mann* [2013a] are likely underestimated for the post 8.4 Ma period.

We note that on Profile 1 (Figure 4) *Fitz and Mann* [2013a] require ~2.3 km of extension since 8.4 Ma within a small graben south of the offshore Goodenough High (e.g., to the west of Goodenough Island, and north of Cape Vogel; see Figure 4), and they also interpret a large basement block underlying the Goodenough High that they suggest is an offshore continuation of the Goodenough Island gneiss dome body. This body is ~20 km wide, and diapiric intrusion of the body into the upper crust may thus have accommodated a further ~20 km of crustal extension, leading to a total extension budget of 22.3 km on our inferred block boundary between Cape Vogel (the Goodenough Bay Block) and the Trobriand Block (Figure 5b). At 5.8 mm/yr from our best fitting model (Figure 5b), this could be accomplished in 3.8 Myr, or over 8.4 Myr at a steady rate of 2.7 mm/yr.

5.2. Evidence for High Slip Rates on Low-Angle Normal Faults

Rock deformation experiments predict that normal faults in frictional Mohr-Coulomb materials such as the upper crust should initiate at steep dips of ~60–70° and that they should frictionally "lock up" at dips <30–45°, depending on the static coefficient of friction [*Axen*, 2004]. The latter predictions are supported by the rarity of global earthquakes rupturing on normal faults dipping at 30° or less [*Collettini*, 2011; *Collettini and Sibson*, 2001]. However, observations of large-displacement low-angle normal faults in the geological record [*Axen*, 2004; *Lister and Davis*, 1989; *Foster and John*, 1999] suggest that low-angle normal faults can indeed accommodate significant plate boundary slip. Resolving this apparent mechanical paradox of the existence of low-angle normal faults remains at the center of a debate about the strength of mature faults [*Rice*, 1992; *Collettini and Sibson*, 2001; *Holdsworth*, 2004; *Carpenter et al*., 2011]. Southeast PNG is one of the best locations on Earth to investigate the mechanics of low-angle normal faulting given the evidence for low-angle normal faulting earthquakes in the Woodlark Rift [*Abers et al*., 1997; *Abers*, 2001], and the well-expressed low-angle (<21° dipping at the surface) detachment fault surface exhumed at the Dayman Dome [e.g.,

Spencer, 2010]. Our GPS results help to place further constraints on the rate at which active low-angle normal faults are slipping.

Motion of the Trobriand Block and Goodenough Bay Block relative to the Papuan Peninsula in our best fitting model yields horizontal slip rates on the Mai'iu Fault of 7–9 mm/yr. There are no other known, active faults in that region, so we assume that the Mai'iu Fault is accommodating all (or most) of the Goodenough/Trobriand Block relative motion. The Mai'iu fault dips at ∼21° near its trace at the base of the Dayman Dome which rises to 2850 m high [*Spencer*, 2010]. The high slip rate we obtain for the Mai'iu fault of 7–9 mm/yr is consistent with the preservation (in a mountainous, high rainfall setting) of the remarkably smooth and striated Dayman Dome exhumed surface, which is a clear indication that the Mai'iu Fault is slipping very rapidly (Figure 2) [*Spencer*, 2010; *Daczko et al*., 2011].

We obtain total extension rates of 17 mm/yr for the structures bounding the Moresby Seamount and the North Moresby Graben (Figure 5), which is well constrained by GPS measurements at sites on the Trobriand Block to the north, and at the GPS site on Strathord Island (STRA), to the south of the Moresby Seamount. *Taylor and Huchon* [2002] suggest 11.5 km of total horizontal extension on the Moresby Seamount (10 km) and north Moresby Graben (1.5 km), one-third of which occurred between 8.4 and 3.8 Ma. Assuming extension rates from GPS of 18 mm/yr, it would take only ∼425 kyr to accommodate the entire 11.5 km, if the modern-day budget of 18 mm/yr was accommodated at the Moresby Seamount and north Moresby Graben. Structures in the south Moresby Graben are thought to be largely inactive [*Goodliffe and Taylor*, 2007], and it is likely that plate boundary deformation has largely coalesced onto the structures bounding the Moresby Seamount and the North Moresby Graben in more recent times. We expect that a focusing of deformation into the Moresby Seamount region may have accompanied the ∼500 kyr reorganization of Woodlark rifting kinematics.

Our new GPS data indicate that slip on active low-angle (20–30° dipping) normal faults (Moresby Seamount and Mai'iu faults) can occur at plate boundary rates that are on the order of 1 cm/yr. The Dayman Dome is the most pristinely expressed of about five active low-angle (<25°) Metamorphic Core Complexes known to exist globally, and it is the only one forming as a "primary" rift fault rather than at a bend in a strike-slip fault system [*Collettini*, 2011; *Spencer*, 2010]. Other known, active low-angle normal faults in continental crust such as those in Italy, the western U.S., and the Aegean undergo slip at rates <3 mm/yr [*Hreinsdottir et al*., 2009; *Niemi et al*., 2004; *Mouslopoulou et al*., 2009]. The process(es) by which such highly misoriented faults may undergo slip remain unresolved. One way of enabling slip on LANFs is to make the fault extremely weak via either pore fluid overpressure and/or low coefficients of friction of the material in the fault zone [e.g., *Sibson*, 1990; *Holdsworth*, 2004], and perhaps also promoting aseismic creep by a stable sliding process. Indirect support for the aseismic creep hypothesis has recently come from experiments on gouges from LANFs that indicate not only low frictional coefficients (<0.2–0.3), but also a velocity-strengthening behavior that is consistent with stable sliding rather than stick slip [*Colletini et al*., 2011; *Ikari et al*., 2012]. Alternatively, others have argued that maximum compressive stress at depth can rotate to an orientation favorable to LANF fault slip [e.g., *Westaway*, 2005]. *Hreinsdottir et al*. [2009] show geodetic evidence for aseismic creep of the Alto Tiberina fault in Italy, supporting the idea that slip on LANFs is promoted by extremely low effective normal stress. It is certainly possible that the Mai'iu fault also undergoes aseismic creep (similar to the Alto Tiberina fault), although our geodetic network is not sufficiently dense in the region of the Mai'iu fault to determine whether or not this is the case.

5.3. Implications for Ultra-High Pressure Rock Exhumation

The recognition of Ultra-High Pressure (UHP) rock terranes which have been exhumed from depths of 90–150 km beneath the Earth's surface have led to one of the most exciting questions in continental dynamics: How do these pieces of continental crust become deeply buried and then subsequently are exhumed? The world's youngest UHP terranes occur in the D'Entrecasteaux Islands and have been exhumed in the last 8–4 million years [*Baldwin et al*., 2004; *Monteleone et al*., 2007]. The D'Entrecasteaux Islands are an important locale to study the mechanism of UHP exhumation, as UHP terranes elsewhere in the world are several to tens of millions of years old, and the overall tectonic boundary conditions that brought them to the surface are not well understood.

Our GPS results record a strong localization of extension in the portion of the rift that hosts the exhumation of these youngest known UHP rocks. They indicate that total extension rates across the D'Entrecasteaux

Islands range from 6 to 12 mm/yr (Figure 5b). This natural laboratory provides compelling evidence that extensional processes can play a major role in the exhumation of UHP rocks [e.g., *Hacker et al*., 2000; *Walsh and Hacker*, 2004], in contrast to other popular models that require collisional and/or subduction-related processes in conjunction with considerable erosion to exhume the UHP terranes [e.g., *Chemenda et al*., 1995].

Two competing models have been proposed for UHP exhumation in the Woodlark Rift: (1) exhumation via buoyancy forces (the diapir model) [*Little et al*., 2011; *Ellis et al*., 2011], and (2) unsubduction or "eversion" of a previously subducted slab via rapid normal faulting on a preexisting suture [*Webb et al*., 2008]. In the diapir model, buoyant rise of a previously subducted fragment of continental crust occurs at the onset of rifting. Results from geodynamic modeling of the diapir process [*Ellis et al*., 2011] agree well with structural geological evidence for vertical ductile thinning (pure shear) in the gneiss domes and ductile flow perpendicular to the plate motion direction [*Little et al*., 2011, 2013]. The geodynamic models also produce localization of extension both off the axis of the rising UHP bodies and within the area of UHP exhumation and gneiss dome emplacement, which agrees well with our GPS results requiring extension in the area of UHP exhumation, as well as on the off-axis Ma'aiu Fault.

While it does not explain the current setting of the UHP rocks exhumed in discrete gneiss domes, the subduction eversion model argues that a suture that once accommodated subduction of the Australian margin beneath PNG has been reactivated as a normal fault, effectively "unsubducting" the Australian margin. To exhume the UHP rocks purely via fault slip in such a short period of time would require extension rates that are well in excess of 20 mm/yr to be focused on a single fault for up to ~8 Myr. We observe 6–12 mm/yr of extension in the D'Entrecasteaux Islands with GPS today, much less than that required to exhume the UHP rocks via eversion. Moreover, the GPS results reveal that this extension is distributed across both sides of the islands (Figure 5; see also *F* tests for models 1 versus 4 and models 1 versus. 7 in Table 4), and not along a single dipping fault as required by the subduction eversion model. Thus, we contend that the GPS results are more compatible with the diapir model for UHP exhumation.

5.4. Constraints on Contemporary Seafloor Spreading Rates at the Woodlark Spreading Center

Figure 7 shows total extension rates for the entire plate boundary inferred from the poles of rotation of *Taylor et al*. [1999] for the two most recent stages of rifting (3.6–0.5 Ma and 0.5 Ma to present), compared with the contemporary GPS rates (derived from the rotation of the Trobriand block relative to the Australian Plate) from our best fitting block model (e.g., Figure 5). We use Trobriand Block/Australian Plate relative motion for the GPS results because although we do not have GPS sites on the Woodlark Plate itself, the Trobriand block motion provides an upper boundary for possible modern-day seafloor spreading rates in the eastern Woodlark Basin. For example, if seafloor spreading rates in the Woodlark Basin are higher than the observed northward motion of the Trobriand Block allows, contraction between the two blocks would occur. Contraction is not observed anywhere in the rift, whereas right-lateral strike slip and extension is well documented along the Woodlark Plate/Trobriand Block boundary from marine geophysical studies and earthquakes [*Abers et al*., 1997; *Taylor et al*., 1999; *Taylor and Huchon*, 2002; *Taylor et al*., 2008a, 2008b; e.g., Moresby Seamount and Nubara Fault; Figure 1].

Thus, using the Trobriand Block/Australian Plate pole of rotation (which gives us the maximum possible extension rate in the Woodlark Basin from GPS), we obtain contemporary extension rates in the seafloor spreading portion near 152°E of 21 mm/yr, increasing eastward to ~40 mm/yr in the eastern portion of the Woodlark Basin (Figure 7). These rates are significantly (up to 50%) lower than those previously derived from the study of magnetic anomalies in the oceanic Woodlark Basin for period between 3.6 and 0.5 Ma [*Taylor et al*., 1999]. The latter predict ~40 mm/yr of extension near 152°E, increasing to ~70 mm/yr in the eastern part of the Woodlark Basin (Figure 7). The 0.5 Ma to present spreading rates are slightly lower than the 3.6–0.5 Ma rates, but are still ~30–50% higher than the GPS rates (Figure 7, compare green and black vectors). The large difference between the GPS-derived rates versus the seafloor spreading-derived rates from *Taylor et al*. [1999] has been a persistent problem in understanding the active tectonics of PNG, as noted by *Tregoning et al*. [1998] and *Wallace et al*. [2004].

To robustly test if the GPS and kinematic data can be fit by the 0.5 Ma to present spreading rates in the Woodlark Rift (green arrows in Figure 7), we conduct an inversion of the GPS and kinematic data by fixing the Woodlark Plate pole to the 0.5 Ma to present pole from *Taylor et al*. [1999]. To fit the GPS data, while fixing the 0.5 Ma to present pole of rotation to that of *Taylor et al*. [1999] requires large contraction (~18 mm/yr) across the boundary between the Trobriand Block and Woodlark Plate southeast of Woodlark Island, due

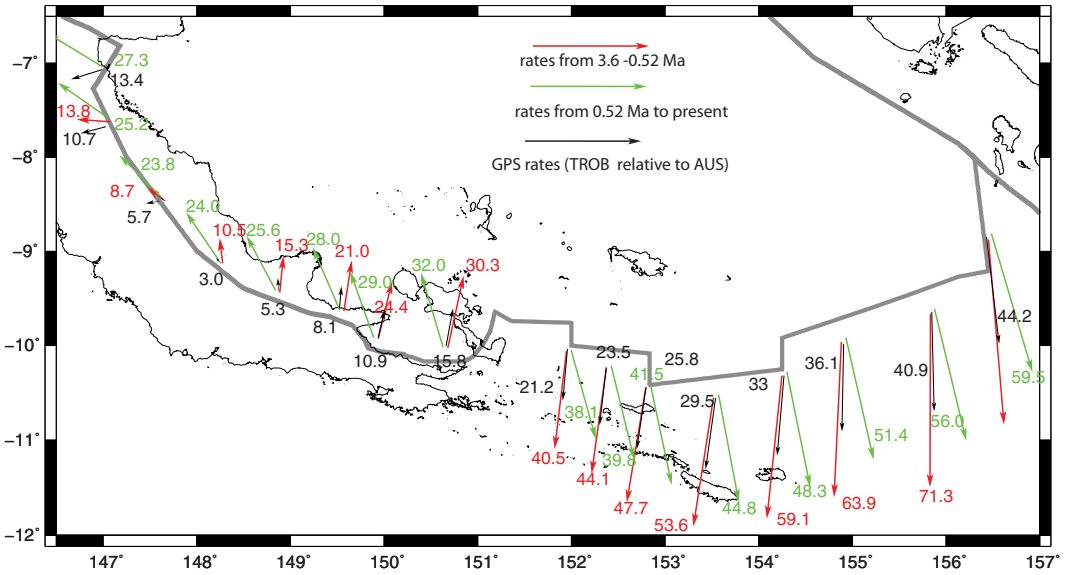

Figure 7. Comparison of total rifting rates (in mm/yr) for the entire plate boundary using Woodlark/Australia poles for 3.6–0.52 Ma (red), 0.52 Ma to present (green) [*Taylor et al*., 1999], and GPS rates for the Trobriand Block relative to Australia (which represents a total extension budget for the area, including Woodlark basin seafloor spreading) from this study.

to the much higher northward rate of motion of the Woodlark Plate of the *Taylor et al*. [1999] pole (Figure 8a). This model also requires contraction on the Nubara Fault (14–18 mm/yr), which is in marked contrast to its observed right-lateral strike-slip behavior (Figure 1) [*Taylor et al*., 2008a, 2008b].

To test if an independent Solomon Sea Plate helps to remedy the situation, we conducted an inversion where we fix the Woodlark Plate pole to the 0.5 Ma to present value [*Taylor et al*., 1999], and allow the Solomon Sea Plate to move independently of the Trobriand Block. In this case, we are able to maintain right-lateral motion on the Nubara Fault (the Solomon Sea/Woodlark Boundary in this model), but to do this requires extension in the Trobriand Trough, as well as contraction southeast of Woodlark Island (Figure 8b). Whether or not the Trobriand Trough accommodates active subduction is unknown, and is one of the most controversial topics in PNG tectonics [*Cooper and Taylor*, 1987; *Abers and Roecker*, 1991]. Our results in Figure 8b suggest that if the Trobriand Trough is an active feature today, it is more likely to be undergoing extension rather than accommodating active subduction. Possible extension at the Trobriand Trough agrees with normal faults identified in seismic reflection data near the Trobriand Trough [*Soto-Cordero*, 1998], as well as the fact that the only shallow (<40 km) earthquake focal mechanism coinciding with the Trobriand Trough from the Global CMT catalog is a normal faulting earthquake (Figure 1). Moreover, if active subduction occurs at the Trobriand Trough (e.g., if the Solomon Sea Plate moves southwest relative to the Trobriand Block), this exacerbates the GPS/seafloor spreading discrepancy even further, as this scenario would result in contraction and left-lateral strike slip along the boundary between the Solomon Sea and Woodlark Plates, and is kinematically inconsistent with geological and seismological observations for right-lateral strike slip on the Nubara Fault (Figure 1, see earthquake focal mechanisms, and *Taylor et al*. [2008a, 2008b]).

One explanation for the difference between the GPS results and the seafloor spreading results of *Taylor et al*. [1999] is that the spreading rate in the Woodlark Rift has decreased by 30–50% over the last 500 kyr, to the current rates (see section 5.5, for a discussion of mechanisms that could lead to the decrease in spreading rates). It is also likely that the 0.5 Ma to present seafloor spreading rates estimated by *Taylor et al*. [1999] are an over-estimate, as they are only based on crust created during the Brunhes (modern) Chron, which began 0.78 Ma. Estimates of spreading rates based only on this period may have large uncertainties, and reinterpretation of the 0.5 Ma to present seafloor spreading rates is warranted in the context of our GPS results.

5.5. Driving Mechanisms of Microplate Rotation and Rifting in the Woodlark Region

Rapid rotation of the overriding plate is common at subduction plate boundaries worldwide, and these rapid fore-arc rotations typically coincide with a transition from collision to subduction [*Wallace et al*., 2005, 2009]. The Woodlark Plate is also undergoing rapid rotation, although in contrast to the upper plate

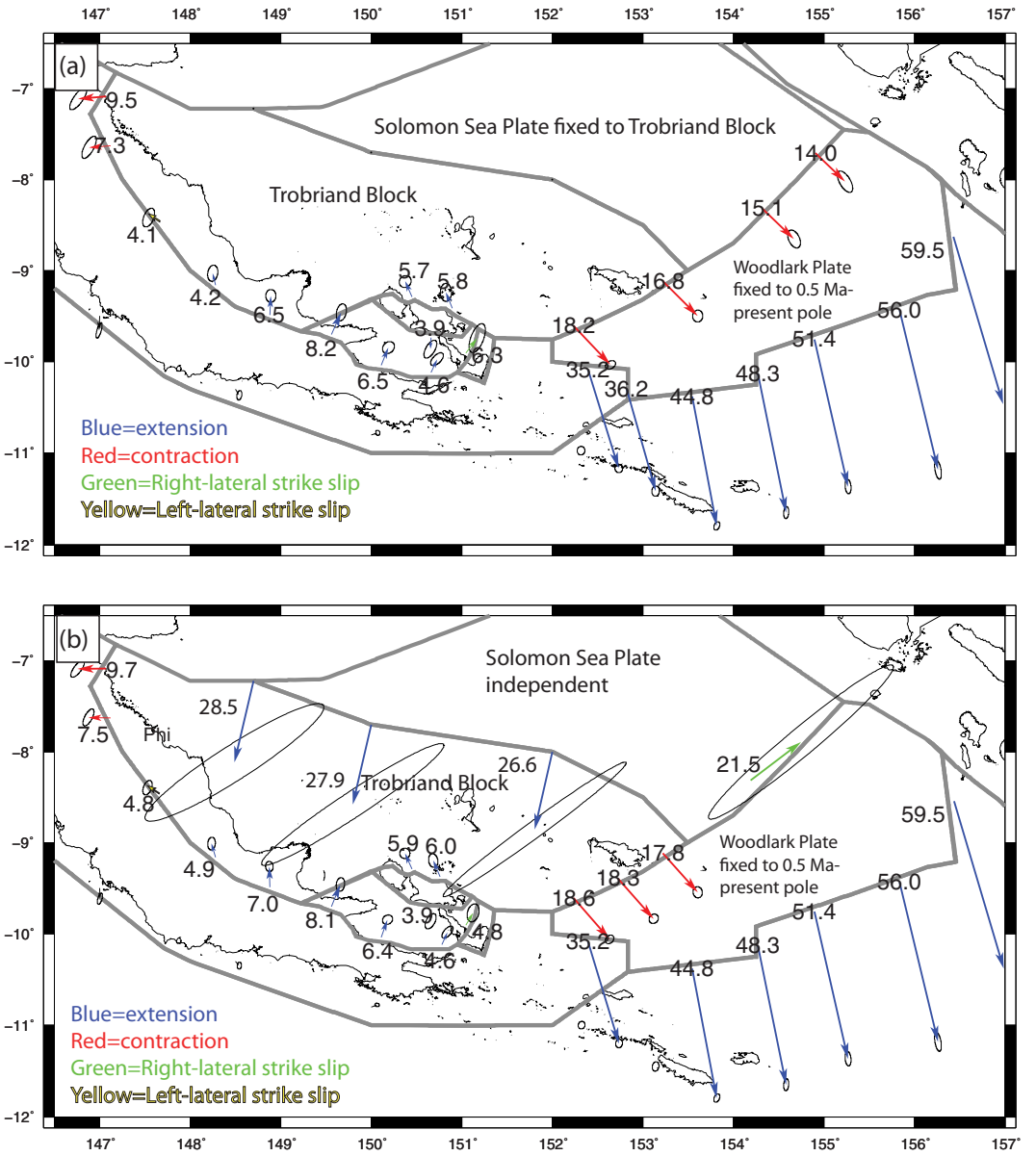

Figure 8. (a) Results of kinematic model where the Woodlark Plate/Australia pole is fixed to the 0.5 Ma to present pole of rotation and the Solomon Sea Plate is fixed to the Trobriand Block (e.g., no relative motion across the Trobriand Trough. (b) Model exactly like that in Figure 8a except that we solve for an independent Solomon Sea Plate pole. Arrows show relative motion of adjacent blocks across their boundaries, with rates labeled in mm/yr. Colors correspond to the type of deformation across that boundary (see keys at bottom left).

examples mentioned above, it is on the lower plate of a subduction zone (the New Britain Trench) (Figure 9). Previous studies have suggested northward motion of the Woodlark Plate and subsequent rifting in southeastern PNG is due to slab pull forces at the New Britain Trench [*Weissel et al.*, 1982; *Wallace et al.*, 2004], where convergence occurs at rates of 10–15 cm/yr, and a long slab has been subducted up to 600 km deep [*Hayes et al.*, 2012] over the last several million years (Figure 9).

Although slab pull forces at the New Britain Trench are a reasonable explanation for rifting in the Woodlark Basin, the cause of rapid rotation of the Woodlark Plate about a nearby pole of rotation (Figure 5c and Table 3) is less clear. We suggest that the along-strike transition from collision of the Finisterre arc terrane with the Australian Margin at the western end of the New Britain Trench (Figure 9) to rapid subduction of the Solomon Sea at the New Britain Trench leads to a situation where the slab pull forces exerted on the Woodlark Plate vary strongly from west to east. The faster northward pull at the eastern New Britain Trench compared to collisional resistance to northward motion of the Woodlark Plate further west, sets up a situation

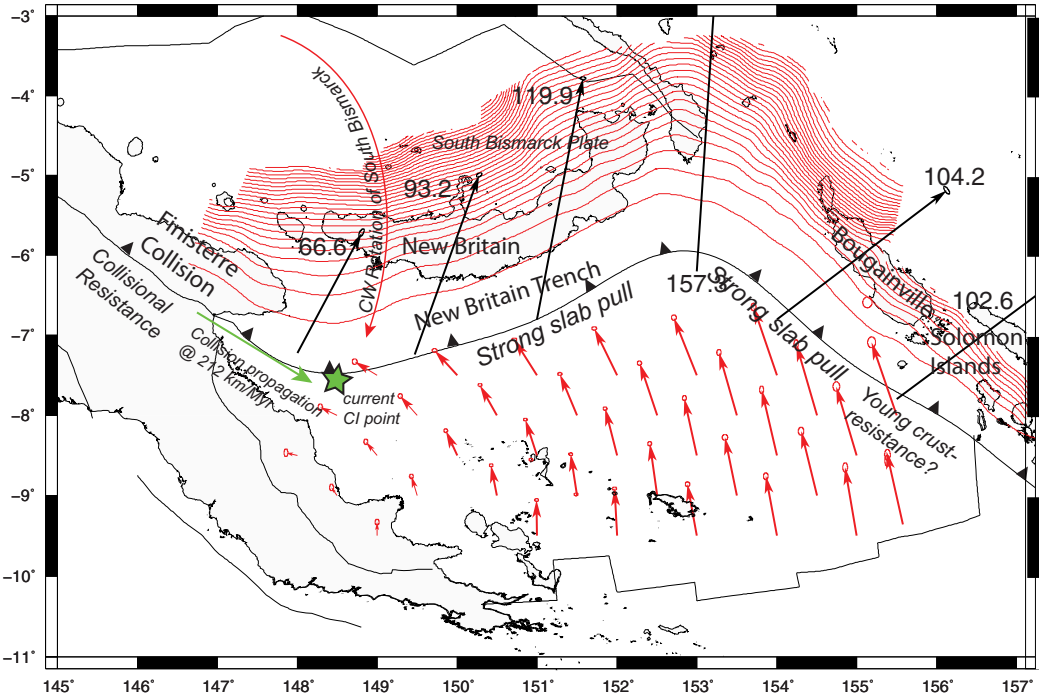

Figure 9. Convergence rates (black arrows, in mm/yr) and slab configuration (red contours) at the New Britain Trench. New Britain slab contours are in 20 km intervals, with the maximum depth shown at 600 km (contours from *Hayes et al*. [2012]). West of 153°E, New Britain Trench rates are determined using Woodlark/South Bismarck Plate relative motion (the South Bismarck pole of rotation is from *Wallace et al*. [2004]), while east of 153°E rates are from Woodlark/Pacific Plate relative motion determined in this study. Red arrows show rotation of the Woodlark and Trobriand blocks relative to the Australian Plate (same scale as for the New Britain Trench rates). Large curved red arrow schematically shows rapid clockwise rotation of the South Bismarck Plate relative to Australia. This rapid clockwise rotation (~8°/Myr) [*Tregoning et al*., 1998; *Wallace et al*., 2004] of the South Bismarck Plate produces the strong eastward increase in convergence rate at the New Britain Trench. Collision initiation propagation shown schematically with green arrow and green star (the modern collision initiation point, after *Silver et al*. [1991]. CI = collision initiation.

where the Woodlark Plate is torqued in an anticlockwise fashion. The Finisterre collision initiation point is propagating rapidly southeast along the plate boundary at a rate of ~212 km/Myr over the last 1 Myr, as the Finisterre Arc terrane "scissors" into the Australian Margin [*Silver et al*., 1991] (Figure 9). This rapid southeastward propagation of the Finisterre Collision has led to large, recent changes in the magnitude of forces acting on the boundaries of the Woodlark Plate, and may explain the recent slowing of Woodlark Basin spreading rates, as discussed above in section 5.4. For example, as the Finisterre Collision encroaches on the region, it will begin to more strongly counteract the northward slab pull forces that dominate at the New Britain Trench further to the east. Resistance to subduction of the recently created Woodlark Basin crust in the eastern Woodlark Spreading Center could also help to produce an overall decrease in forces driving northward motion of the Woodlark Plate, and contribute to a slowing of Woodlark spreading/rifting rates (Figures 1 and 9).

The role of slab pull forces at the New Britain Trench also has implications for the nature of deformation at the Trobriand Trough, a topic of considerable controversy [e.g., *Cooper and Taylor*, 1987; *Abers and Roecker*, 1991]. We contend that the strong northward pull from the subducted slab at the New Britain Trench induces extensional stresses across the Solomon Sea Plate and Trobriand Trough. Such a situation would make it difficult to sustain forces driving convergence at the Trobriand Trough; instead, we expect that if the Trobriand Trough is a currently active plate boundary, that it is more likely to be undergoing extension (see also discussion in section 5.4). However, we do agree that the Trobriand Trough may have accommodated active subduction in the past, perhaps up until the Miocene when rifting began in southeast PNG.

6. Conclusions

The Woodlark Rift in southeast PNG provides a globally unique natural laboratory to investigate an array of processes, including: continental breakup and seafloor spreading, slip on low-angle normal faults, and

exhumation of Ultra-High Pressure rocks. Our results from a network of 45 campaign GPS sites in southeastern PNG place new constraints on the overall rates of rifting in the continental and oceanic portions of the Woodlark Rift, which range from several mm/yr in the western rift, up to ~40 mm/yr in the eastern portion of the Woodlark Spreading Center. The strong gradation in extension rates is related to rapid rotation of the Woodlark Plate and Trobriand Block (at 2–2.7°/Myr) about nearby poles of rotation.

In the continental portion of the rift, where our GPS network is more concentrated, the plate boundary deformation is distributed across several structures. At least half of the extension budget is concentrated in the D'Entrecasteaux Islands, a region of actively exhuming Ultra-High Pressure rock terranes, indicating that extensional processes may play a major role in the exhumation of UHP terranes [e.g., *Hacker et al*., 2000; *Walsh and Hacker*, 2004; *Ellis et al*., 2011]. We also find that a low-angle normal fault (LANF), the Mai'iu fault, is a primary plate boundary feature slipping at a rate of at least several mm/yr, and that the ~30° dipping fault bounding the Moresby Seamount is slipping at rates as high as 17 mm/yr. These are the highest slip rates ever documented for LANFs worldwide, and our GPS results confirm that LANFs can indeed undergo slip at high rates (e.g., several mm/yr or more). In the continental portion of the Woodlark rift, our GPS deformation rates agree well with geological studies of *Kington and Goodliffe* [2008] in the area of the Moresby Seamount, while farther to the west the GPS indicate overall higher rates of deformation than those inferred from geological data by *Fitz and Mann* [2013a].

Although our GPS network does not allow us to directly measure extension rates in the Woodlark Spreading Center (due to the lack of GPS sites on the Woodlark Plate), we argue that our results do place an upper bound on possible spreading rates there. Overall, the GPS rates of seafloor spreading are 30–50% slower than those determined from magnetic anomalies during the Brunhes Chron (0.78 Myr to present), and are 45–55% slower than spreading rates from 3.8 to 0.5 Ma [*Taylor et al*., 1999]. We suggest that the rates of seafloor spreading in the Woodlark Rift have decreased since 3.8 Ma to present-day rates. It is also likely that the Brunhes Chron rates are in error since they are based on a shorter period of seafloor spreading (e.g., the last 0.78 Myr), and the 0.5 Ma to present seafloor spreading rates may be overestimated, and should be reinterpreted in the context of the GPS. If there has been a recent decrease in spreading rates, this may be related to southeastward propagation of the Finisterre arc-continent collision on the northern boundary of the Woodlark/Solomon Sea Plate. Southeast propagation of the Finisterre collision provides resistance to northward motion of the Woodlark plate, by counteracting the strong slab pull forces at the New Britain Trench that are the likely driver of rifting in southeastern PNG.

Acknowledgments

GPS velocities used here are provided in Table 1, and earthquake slip vectors and Defnode input files can be made available upon request. The Marsden Fund of the Royal Society of New Zealand provided the funding for this project. We appreciate constructive reviews by Associate Editor Geoff Abers and two anonymous reviewers. We are indebted to the crew of the MV Jazz II, the MV Sara Lee, and the MV Laduwa for their excellent work in transporting us to many of the GPS sites. We thank Geoff Abers for facilitating some of the GPS measurements in 2010 during their seismic deployments. We thank Guy Fitz and Paul Mann for sharing some of their figures for modification in this paper. We are grateful for assistance in the field during the 2012 campaign from Sibona Kila and Ghana Manhi from the University of Technology in Lae, and to George Aigoma, Ebo Thomas, and Joel Mitchell for assistance in 2009. Ben Yawai, Willie Solomon, and Nielsen Panta provided important logistical and surveying support in Alotau. Most importantly, we acknowledge the assistance of countless individuals in southeastern PNG. Without their hospitality and goodwill, this work would not have been possible.

References

Abers, G. A. (2001), Evidence for seismogenic normal faults at shallow depths in continental rifts, in *Non-Volcanic Rifting of Continental Margins*, vol. 187, edited by R. C. L. Wilson et al., pp. 305–318, Geol. Soc., London, U. K.

Abers, G. A., and S. W. Roecker (1991), Deep structure of an arc-continent collision: Earthquake relocation and inversion for upper mantle P and S wave velocities beneath Papua New Guinea, *J. Geophys. Res.*, *96*, 6379–6401.

Abers, G. A., C. Z. Mutter, and J. Fang (1997), Shallow dips of normal faults during rapid extension: Earthquakes in the Woodlark-D'Entrecasteaux rift system, Papua New Guinea, *J. Geophys. Res.*, *102*, 15,301–15,317.

Abers, G. A., et al. (2002), Mantle compensation of active metamorphic core complexes at Woodlark rift in Papua New Guinea, *Nature*, *418*, 862–865.

Altamimi, Z., X. Collilieux, and L. Metivier (2011), ITRF2008: An improved solution of the international terrestrial reference frame, *J. Geod.*, *85*, 457–473.

Axen, G. J. (2004), Low-angle normal fault mechanics and crustal strength, in *Rheology and Deformation of the Lithosphere*, edited by G. Karner, pp. 46–91, Columbia Univ. Press, N. Y.

Baldwin, S. L., B. Monteleone, L. E. Webb, P. G. Fitzgerald, M. Grove, and J. Hill (2004), Pliocene eclogite exhumation at plate tectonic rates in eastern Papua New Guinea, *Nature*, *431*, 263–267, doi:10.1038/nature02846.

Baldwin, S. L., L. E. Webb, and B. D. Monteleone (2008), Late Miocene coesite-eclogite exhumed in the Woodlark Rift, *Geology*, *36*, 735–738.

Bendick, R., S. McClusky, R. Bilham, L. Asfaw, and S. Klemperer (2006), Distributed Nubia-Somalia relative motion and dike intrusion in the Main Ethiopian Rift, *Geophys. J. Int.*, *165*, 303–310, doi:10.1111/j.1365-246X.2006.02904.x.

Benes, V., S. D. Scott, and R. A. Binns (1994), Tectonics of rift propagation into a continental margin: Western Woodlark Basin, Papua New Guinea, *J. Geophys. Res.*, *99*, 4439–4455.

Bialas, R. W., W. R. Buck, and R. Qin (2010), How much magma is required to rift a continent?, *Earth Planet. Sci. Lett.*, *292*, 68–78, doi: 10.1016/j.epsl.2010.01.021.

Boehm, J., B. Werl, and H. Schuh (2006), Troposphere mapping functions for GPS and very long baseline interferometry from European Centre for Medium-Range Weather Forecasts operational analysis data, *J. Geophys. Res.*, *111*, B02406, doi:10.1029/2005JB003629.

Buck, W. R. (2006), The role of magma in the development of the Afro-Arabian rift system, in *The Afar Volcanic Province Within the East African Rift System*, edited by G. Yirgu, C. J. Ebinger, and P. K. H. Maguire, pp. 43–54, Geol. Soc., London, U. K.

Buck, W. R. (2007), The dynamics of continental break-up and extension, in *The Treatise on Geophysics*, edited by A. B. Watts, vol. 6, pp. 335–376, Crustal and Lithosphere Dynamics, Columbia University, Palisades, N. Y.

Cairns, E., T. A. Little, G. M. Turner, L. Wallace, and S. Ellis (2013), Paleomagnetic constraints on vertical-axis rotations in the active Woodlark Rift, SE Papua New Guinea, in *Abstracts, Geosciences 2013 Conference, Christchurch, New Zealand Geosci. Soc. of N. Z. Misc. Publ. 136A*, edited C. M. by Reid and A. Wandres, p. 13, Geoscience Society of New Zealand, New Zealand.

Carpenter, B. M., C. Marone, and D. M. Saffer (2011), Weakness of the San Andreas Fault revealed by samples from the active fault zone, *Nat. Geosci.*, *4*, 251–254.

Chemenda, A. I., M. Mattauer, J. Malavielle, and A. N. Bokun (1995), A mechanism for syn-collisional rock exhumation and associated normal faulting: Results from physical modeling, *Earth Planet. Sci. Lett.*, *132*, 225–232.

Colletini, C. (2011), The mechanical paradox of low-angle normal faults: Current understanding and open questions, *Tectonophysics*, *510*, 253–268.

Collettini, C., and R. H. Sibson (2001), Normal faults, normal friction?, *Geology*, *29*, 927–930.

Colletini, C., A. Niemeijer, C. Viti, S. A. F. Smith, and C. Marone (2011), Fault structure, frictional properties and mixed-mode slip behavior, *Earth Planet. Sci. Lett.*, *311*, 316–327.

Cooper, P., and B. Taylor (1987), Seismotectonics of New Guinea: A model for arc reversal following arc-continent collision, *Tectonics*, *6*, 53–67.

Daczko, N. R., P. Caffi, and P. R. Mann (2011), Structural evolution of the Dayman dome metamorphic core complex, eastern Papua New Guinea, *Geol. Soc. Am. Bull.*, *123*, 2335–2351.

Davies, H. L. (2012), The geology of New Guinea—The cordilleran margin of the Australian continent, *Episodes*, *35*(1), 87–102.

Davies, H. L., and A. L. Jaques (1984), Emplacement of ophiolite in Papua New Guinea, in *Ophiolites and Oceanic Lithosphere, Geol. Soc. Spec. Publ.*, vol. 13, edited by I. G. Gass, S. J. Lippard, and A. W. Shelton, pp. 341–350, The Geological Society, London, U. K.

Davies, H. L., and R. G. Warren (1988), Origin of eclogite-bearing, domed, layered metamorphic complexes ("core complexes") in the D'Entrecasteaux islands, Papua New Guinea, *Tectonics*, *7*, 1–21.

Davies, H. L., and R. G. Warren (1992), Eclogites of the D'Entrecasteaux Islands, *Contrib. Mineral. Petrol.*, *112*, 463–474.

Davies, H. L., and A. N. Williamson (1998), Buna, Papua New Guinea, 1:250,000 Geological Series, *Geol. Surv. of Papua New Guinea Explanatory Notes SC/55-3*, Port Moresby, Papua New Guinea.

Davies, H., J. Lock, D. Tiffin, E. Honza, Y. Okuda, F. Murakami, and K. Kisimoto (1987), Convergent tectonics in the Huon Peninsula region, Papua New Guinea, *Geo Mar. Lett.*, *7*, 143–152.

Dieck, C. C. M., G. A. Abers, Z. Eilon, J. B. Gaherty, and R. Verave (2013), Seismicity in an active rift exposing ultra-high pressure metamorphic rocks: D'Entrecasteaux Islands, Papua New Guinea, Abstract T21A-2524 presented at the 2014 AGU Fall meeting, AGU, San Francisco, Calif.

Dow, D. B. (1977), A geological synthesis of Papua New Guinea, *Bull. Bur. Miner. Resour. Aust.*, *201*, 1–41.

Dziewonski, A. M., and D. L. Anderson (1981), Preliminary reference Earth model, *Phys. Earth Planet. Inter.*, *25*(4), 297–356.

Dziewonski, A. M., T.-A. Chou, and J. H. Woodhouse (1981), Determination of earthquake source parameters from waveform data for studies of global and regional seismicity, *J. Geophys. Res.*, *86*, 2825–2852, doi:10.1029/JB086iB04p02825.

Eilon, Z., G. A. Abers, G. Jin, and J. B. Gaherty (2014), Anisotropy beneath a highly extended continental rift, *Geochem. Geophys. Geosyst.*, *15*, 545–564, doi:10.1002/2013GC005092.

Ekström, G., M. Nettles, and A. M. Dziewonski (2012), The global CMT project 2004–2010: Centroid-moment tensors for 13,017 earthquakes, *Phys. Earth Planet. Inter.*, *200–201*, 1–9, doi:10.1016/j.pepi.2012.04.002.

Ellis, S. M., T. A. Little, L. M. Wallace, B. R. Hacker, and S. J. H. Buiter (2011), Feedback between rifting and diapirism can exhume ultrahigh-pressure rocks, *Earth Planet. Sci. Lett.*, *311*, 427–438, doi:10.1016/j.epsl.2011.09.031.

Epard, J. L., and A. Steck (2008), Structural development of the Tso Morari ultra-high pressure nappe of the Ladakh Himalaya, *Tectonophysics*, *451*, 242–264.

Feigl, K., et al. (1993), Space geodetic measurements of crustal deformation in central and southern California, 1984–1992, *J. Geophys. Res.*, *98*, 21,677–21,712.

Ferris, A., G. A. Abers, B. Zelt, B. Taylor, and S. Roecker (2006), Crustal structure across the transition from rifting to spreading: The Woodlark rift system of Papua New Guinea, *Geophys. J. Int.*, *166*, 622–634.

Fitz, G., and P. Mann (2013a), Evaluating upper versus lower crustal extension through structural reconstructions and subsidence analysis of basins adjacent to the D'Entrecasteaux Islands, eastern Papua New Guinea, *Geochem. Geophys. Geosyst.*, *14*, 1800–1818, doi:10.1002/ggge.20123.

Fitz, G., and P. Mann (2013b), Tectonic uplift mechanism of the Goodenough and Fergusson Island gneiss domes, eastern Papua New Guinea: Constraints from seismic reflection and well data, *Geochem. Geophys. Geosyst.*, *14*, 3969–3995, doi:10.1002/ggge.20208.

Foster, D. A., and B. E. John (1999), Quantifying tectonic exhumation in an extensional orogen with thermochronology: Examples from the southern Basin and Range Province, *Geol. Soc. Spec. Publ.*, *154*, 343–364.

Furlong, K. P., T. Lay, and C. J. Ammon (2009), A great earthquake rupture across a rapidly evolving three-plate boundary, *Science*, *324*, 226–229.

Goldsworthy, M., J. Jackson, and J. Haines (2002), The continuity of active fault systems in Greece, *Geophys. J. Int.*, *148*, 596–618.

Goodliffe, A. M. (1998), The rifting of continental and oceanic lithosphere: Observations from the Woodlark Basin, PhD thesis, Univ. of Hawaii at Manoa, Honolulu.

Goodliffe, A. M., and B. Taylor (2007), The boundary between continental rifting and seafloor spreading in the Woodlark Basin, Papua New Guinea, in *Imaging, Mapping and Modelling Continental Lithosphere Extension and Breakup*, vol. 282, edited by G. D. Karner, G. Manatschal, and L. M. Pinhiero, pp. 213–234, Geol. Soc., London, U. K.

Goodliffe, A. M., B. Taylor, F. Martinez, R. Hey, K. Maeda, and K. Ohno (1997), Synchronous reorientation of the Woodlark Basin Spreading Center, *Earth Planet. Sci. Lett.*, *146*(1), 233–242.

Gordon, S. M., T. A. Little, B. R. Hacker, S. A. Bowring, M. Korchinski, S. L. Baldwin, A. R. C. Kylander-Clark, and M.-A. Millet (2012), Multi-stage exhumation of young UHP-HP rocks: Timescales of melt crystallization in the D'Entrecasteaux Islands, southeastern Papua New Guinea, *Earth Planet. Sci. Lett.*, *351–352*, 237–246.

Hacker, B. (2007), Ascent of the ultra-high pressure Western Gneiss Region, Norway, *Spec. Pap. Geol. Soc. Am.*, *419*, 14.

Hacker, B. R., et al. (2000), Exhumation of UHP continental crust in east-central China: Late Triassic-Early Jurassic tectonic unroofing, *J. Geophys. Res.*, *105*, 13,339–13,364.

Hall, R., and W. Spakman (2002), Subducted slabs beneath the eastern Indonesia-Tonga region: Insights from tomography, *Earth Planet. Sci. Lett.*, *201*, 321–336.

Hayes, G. P., D. J. Wald, and R. L. Johnson (2012), Slab 1.0: A three-dimensional model of global subduction zone geometries, *J. Geophys. Res.*, *117*, B01302, doi:10.1029/2011JB008524.

Herring, T., B. King, and S. McClusky (2010a), *GAMIT Reference Manual*, 10.4, Mass. Inst. of Technol., Cambridge, Massachusetts.

Herring, T., B. King, and S. McClusky (2010b), *GLOBK Reference Manual*, 10.4, Mass. Inst. of Technol., Cambridge, Mass.
Herring, T. A., J. L. Davis, and I. I. Shapiro (1990), Geodesy by radio interferometry: The application of Kalman filtering to the analysis of very long baseline interferometry data, *J. Geophys. Res.*, *95*, 12,561–12,581.
Hill, E. J. (1994), Geometry and kinematics of shear zones formed during continental extension in eastern Papua New Guinea, *J. Struct. Geol.*, *16*, 1093–1105.
Holdsworth, R. E. (2004), Weak faults, rotten cores, *Science*, *303*, 181–182.
Hreinsdottir, S., and R. A. Bennett (2009), Active aseismic creep on the Alto Tiberina low-angle normal fault, Italy, *Geology*, *37*, 683–686.
Ikari, M. J., C. Marone, and D. M. Saffer (2012), On the relation between fault strength and frictional stability, *Geology*, *39*, 83–86.
Jónsson, S., P. Einarsson, and F. Sigmundsson (1997), Extension across a divergent plate boundary, the Eastern Volcanic Rift Zone, south Iceland, 1967–1994, observed with GPS and electronic distance measurements, *J. Geophys. Res.*, *102*, 11,913–11,929, doi:10.1029/96JB03893.
Kington, J. D., and A. M. Goodliffe (2008), Plate motions and continental extension at the rifting to spreading transition in Woodlark Basin, Papua New Guinea: Can oceanic plate kinematics be extended into continental rifts?, *Tectonophysics*, *458*, 82–95.
Kirchoff-Stein, K. S. (1992), Seismic reflection study of the New Britain and Trobriand subduction systems and their zone of initial contact in the western Solomon Sea, PhD thesis, Univ. of Calif., Santa Cruz.
Lavier, L. L., and G. Manatschal (2006), A mechanism to thin the continental lithosphere at magma-poor margins, *Nature*, *440*, 324–328.
Lister, G. S., and G. A. Davis (1989), The origin of metamorphic core complexes and detachment faults formed during Tertiary continental extension in the northern Colorado River region, U.S.A, *J. Struct. Geol.*, *11*, 65–94.
Little, T. A., S. L. Baldwin, P. G. Fitzgerald, and B. Monteleone (2007), Continental rifting and metamorphic core complex formation ahead of the Woodlark Spreading Ridge, D'Entrecasteaux Islands, Papua New Guinea, *Tectonics*, *26*, TC1002, doi:10.1029/2005TC001911.
Little, T. A., B. R. Hacker, S. M. Gordon, S. L. Baldwin, P. G. Fitzgerald, S. Ellis, and M. Korchinski (2011), Diapiric exhumation of the world's youngest (UHP) eclogites in the gneiss domes of the D'Entrecasteaux Islands Papua New Guinea, *Tectonophysics*, *510*(1–2), 39–68, doi:10.1016/j.tecto.2011.06.006.
Little, T. A., B. R. Hacker, S. Brownlee, and G. Seward (2013), Microstructures and quartz lattice preferred orientations in the eclogite-bearing migmatitic gneisses of the D'Entrecasteaux Islands, Papua New Guinea, *Geochem. Geophys. Geosyst.*, *14*, 2030–2062, doi:10.1002/ggge.20132.
Lus, W. Y., I. McDougall, and H. L. Davies (2004), Age of the metamorphic sole of the Papuan Ultramafic Belt ophiolite, Papua New Guinea, *Tectonophysics*, *392*, 85–101.
Mao, A., C. G. A. Harrison, and T. H. Dixon (1999), Noise in the GPS coordinate time series, *J. Geophys. Res.*, 104, 2797–2816.
Martinez, F., A. Goodliffe, and B. Taylor (2001), Metamorphic core complex formation by density inversion and lower crustal extrusion, *Nature*, *411*, 930–933.
McCaffrey, R. (2002), Crustal block rotations and plate coupling, in *Plate Boundary Zones,* vol. 30, *AGU Geodyn. Ser.*, edited by S. Stein and J. Freymueller, pp. 100–122, American Geophysical Union, Washington, D. C.
McClusky, S., et al. (2000), Global Positioning System constraints on plate kinematics and dynamics in the eastern Mediterranean and Caucasus, *J. Geophys. Res.*, *105*, 5695–5719.
Miller, S. R., S. L. Baldwin, and P. G. Fitzgerald (2012), Transient fluvial incision and active surface uplift in the Woodlark Rift of eastern PNG, *Lithosphere*, *4*(2), 131–149, doi:10.1130/L135.1.
Monteleone, B. D., S. L. Baldwin, L. E. Webb, P. G. Fitzgerald, M. Grove, and A. K. Schmitt (2007), Late Miocene-Pliocene eclogite-facies metamorphism, D'Entrecasteaux Islands, SE Papua New Guinea, *J. Metamorph. Geol.*, *25*, 245–265.
Mouslopoulou, V., J. J. Walsh, and A. Nicol (2009), Fault displacement rates on a range of timescales, *Earth Planet. Sci. Lett.*, *278*, 186–197.
Mutter, J. C., C. Z. Mutter, and J. Fang (1996), Analogies to oceanic behaviour in the continental breakup of the western Woodlark basin, *Nature*, *380*, 333–336.
Niemi, N. A., B. P. Wernicke, A. M. Friedrich, M. Simons, R. A. Bennett, and J. L. Davis (2004), BARGEN continuous GPS data across the eastern Basin and Range province, and implications for fault system dynamics, *Geophys. J. Int.*, *159*, 842–862, doi:10.1111/j.1365-246X.2004.02454.x.
Okada, Y. (1985), Surface deformation to shear and tensile faults in a halfspace, *Bull. Seismol. Soc. Am.*, *75*, 1135–1154.
Ollier, C. D., and C. F. Pain (1980), Actively rising surficial gneiss domes in Papua New Guinea, *J. Geol. Soc. Aust.*, *27*, 33–44.
Pollitz, F. F. (1996), Coseismic deformation from earthquake faulting on a layered spherical Earth, *Geophys. J. Int.*, *125*(1), 1–14.
Press, W. H., B. P. Flannery, S. A. Teukolsky, and W. T. Vetterling (1989), *Numerical Recipes*, Cambridge Univ. Press, Cambridge, U. K.
Reston, T. (2007), Extension discrepancy at North Atlantic nonvolcanic rifted margins: Depth-dependent stretching or unrecognized faulting?, *Geology*, *35*(4), 367–270.
Rice, J. R. (1992), Fault stress states, pore pressure distributions, and the weakness of the San Andreas fault, in *Fault Mechanics and Transport Properties of Rocks: A Festschrift in Honor of W.F. Brace*, edited by B. Evans and T. F. Wong, pp. 475–503, Academic Press, San Diego, Calif.
Savage, J. C. (1983), Dislocation model of strain accumulation and release at a subduction zone, *J. Geophys. Res.*, *88*, 4984–4996.
Sibson, R. H. (1990), Conditions for fault-valve behavior, in *Deformation Mechanisms, Rheology, and Tectonics*, vol. 54, edited by R. J. Knipe and E. H. Rutter, pp. 15–28, Geol. Soc. London, Spec. Publ., London, U. K.
Silver, E. A., L. D. Abbott, K. S. Kirchoff-Stein, D. L. Reed, B. Bernstein-Taylor, and D. Hilyard (1991), Collision propagation in Papua New Guinea and the Solomon Sea, *Tectonics*, *10*, 863–874.
Smith, I. E., and H. L. Davies (1976), Geology of the southeast Papuan Mainland, *BMR J. Aust. Geol. Geophys.*, *165*, 32.
Smith, I. E. M. (1982), Volcanic evolution of Eastern Papua, *Tectonophysics*, *87*, 315–333.
Smith, I. E. M., and J. S. Milsom (1984), Late Cenozoic volcanism and extension in the eastern Papua, in *Marginal Basin Geology*, edited by B. P. Kokelaar and M. F. Howells, pp. 163–171, The Geological Society, London, U. K.
Soto-Cordero, L. (1998), Crustal processes associated with two slow convergent systems: The Trobriand trough, Papua New Guinea and the northern Panama deformed belt, MS thesis, 56 pp., Univ. of California, Santa Cruz, Calif.
Speckbacher, R., J. H. Behrmann, T. J. Nagel, M. Stipp, and C. W. Devey (2011), Splitting a continent: Insights from submarine high-resolution mapping of the Moresby Seamount detachment, offshore Papua New Guinea, *Geology*, *39*(7), 651–654.
Spencer, J. E. (2010), Structural analysis of three extensional detachment faults with data from the 2000 Space-Shuttle Radar Topography Mission, *GSA Today*, *20*(8), 1–10.
Stearns, M. A., B. R. Hacker, L. Ratschbacher, J. Lee, J. M. Cottle, and A. Kylander-Clark (2013), Synchronous Oligocene-Miocene metamorphism of the Pamir and the North Himalaya driven by plate-scale dynamics, *Geology*, *41*, 1071–1074.

Taylor, B., and N. F. Exon (1987), An investigation of ridge subduction in the Woodlark-Solomons region: Introduction and overview, in *Marine Geology, Geophysics and Geochemistry of the Woodlark Basin-Solomon Islands, Circum-Pac. Counc. for Energy and Miner. Resour. Earth Sci. Ser.*, edited by B. Taylor and N. F. Exon, pp. 1–24, Houston, Tex.

Taylor, B., and P. Huchon (2002), Active continental extension in the western Woodlark Basin: a synthesis of Leg 180 results, in *Proceedings of the Ocean Drilling Program, Scientific Results* [CD ROM], vol. 180, edited by P. Huchon, B. Taylor, and A. Klaus, pp. 1–36, Ocean Drill. Prog., Texas A&M Univ., College Station, Tex.

Taylor, B., A. M. Goodliffe, and F. Martinez (1999), How Continents break-up: Insights from Papua New Guinea, *J. Geophys. Res.*, *104*, 7497–7512.

Taylor, B., A. Goodliffe, and F. Martinez (2008a), Initiation of transform faults at rifted continental margins, *C. R. Geosci.*, *341*, 428–438, doi: 10.1016/j.crte.2008.08.010.

Taylor, F. W., R. W. Briggs, C. Frolhlich, A. Brown, M. Hornbach, A. K. Papabatu, A. J. Meltzner, and D. Billy (2008b), Rupture across arc segment and plate boundaries in the 1 April 2007 Solomons earthquake, *Nat. Geosci.*, *1*, 253–257.

Tregoning, P., and C. Watson (2009), Atmospheric effects and spurious signals in GPS analyses, *J. Geophys. Res.*, *114*, B09403, doi:10.1029/2009JB006344.

Tregoning, P., and C. Watson (2011), Correction to "Atmospheric effects and spurious signals in GPS analyses," *J. Geophys. Res.*, *116*, B02412, doi:10.1029/2010JB008157.

Tregoning, P., et al. (1998), Estimation of current plate motions in Papua New Guinea from Global Positioning System observations, *J. Geophys. Res.*, *103*, 12,181–12,203.

Tregoning, P., R. Burgette, S. C. McClusky, S. Lejeune, C. S. Watson, and H. McQueen (2013), A decade of horizontal deformation from great earthquakes, *J. Geophys. Res.*, *118*, 2371–2381, doi:10.1002/jgrb.50154.

van Ufford, Q. A., and M. Cloos (2005), Cenozoic tectonics of New Guinea, *Am. Assoc. Petrol. Geol. Bull.*, *89*, 119–140.

van Wijk, J. W., and D. K. Blackman (2005), Dynamics of continental rift propagation: The endmember modes, *Earth Planet. Sci. Lett.*, *229*, 247–258.

van Wijk, J. W., R. S. Huismans, M. ter Voorde, and S. A. P. L. Cloetingh (2001), Melt generation at volcanic continental margins: No need for a mantle plume?, *Geophys. Res. Lett.*, *28*(20), 3995–3998.

Wallace, L. M., et al. (2004), GPS and seismological constraints on active tectonics and arc-continent collision in Papua New Guinea: Implications for mechanics of microplate rotations in a plate boundary zone, *J. Geophys. Res.*, *109*, B05404, doi:10.1029/2003JB002481.

Wallace, L. M., R. McCaffrey, J. Beavan, and S. Ellis (2005), Rapid microplate rotations and back-arc rifting at the transition between collision and subduction, *Geology*, *33*(11), 857–860.

Wallace, L. M., S. Ellis, and P. Mann (2009), Collisional model for rapid fore-arc block rotations, arc curvature, and episodic back-arc rifting in subduction settings, *Geochem. Geophys. Geosyst.*, *10*, Q05001, doi:10.1029/2008GC002220.

Walsh, E. O., and B. Hacker (2004), The fate of subducted continental margins: Two-stage exhumation of the HP to UHP Western Gneiss Complex, Norway, *J. Metamorph. Geol.*, *22*, 671–689.

Webb, L. E., S. L. Baldwin, T. A. Little, and P. G. Fitzgerald (2008), Can microplate rotation drive subduction inversion?, *Geology*, *36*, 823–826.

Weissel, J. K., B. Taylor, and G. D. Karner (1982), The opening of the Woodlark Basin, subduction of the Woodlark spreading system, and the evolution of northern Melanesia since mid-Pliocene time, *Tectonophysics*, *87*, 253–277.

Westaway, R. (2005), Active low-angle normal faulting in the Woodlark extensional province, Papua New Guinea: A physical model, *Tectonics*, *24*, TC6003, doi:10.1029/2004TC001744.

White, R. S., and D. P. McKenzie (1989), Magmatism at rift zones: The generation of volcanic continental margins and flood basalts, *J. Geophys. Bull.*, *94*, 7685–7729.

Zirakparvar, N. A., S. L. Baldwin, and J. D. Vervoort (2013), The origin and geochemical evolution of the Woodlark Rift of Papua New Guinea, *Gondwana Res.*, *23*, 931–943.